https://doi.org/10.5194/cp-2021-59
Preprint. Discussion started: 2 June 2021

Climate of the Past Discussions

Holocene paleoceanography of the Northeast Greenland shelf

Teodora Pados-Dibattista[1], Christof Pearce[1], Henrieka Detlef[1], Jørgen Brendtsen[2], Marit-Solveig Seidenkrantz[1]

[1]Department of Geoscience, Aarhus University, Aarhus, 8000, Denmark
[2]Norwegian Institute for Water Research (NIVA), Copenhagen, 2300, Denmark

Correspondence to: Teodora Pados-Dibattista (pados.theo@gmx.at) and Marit-Solveig Seidenkrantz (mss@geo.au.dk)

Abstract. The Northeast Greenland shelf is highly sensitive to climate and ocean variability because it is swept by the East Greenland Current, which, through the western Fram Strait, forms the main pathway of export of sea ice and cold water masses from the Arctic Ocean into the North Atlantic Ocean. We carried out benthic foraminiferal assemblage, stable isotope- and sedimentological analyses of a marine sediment core retrieved from the Northeast Greenland shelf (core DA17-NG-ST7-73), which provided a multiproxy reconstruction of Holocene paleoceanographic conditions. The results reveal significant variations in the water masses and thus, in the strength of the East Greenland Current over the last ca. 9.4 ka BP. Between 9.4 and 8.2 ka BP the water column off Northeast Greenland was highly stratified, with cold, sea ice-loaded surface waters and strong influx of warm Atlantic Water in the subsurface. At ~8.4 ka BP a short-lived peak in terrestrial elements may be linked to influx of ice-berg transported sediments and thus, to the so-called 8.2 ka event. Holocene Thermal Maximum like conditions prevailed from 8.2 to 6.2 ka BP, with a strong influence of the Return Atlantic Current and a weakened transport of Polar Water in the upper East Greenland Current. After 6.2 ka BP we recorded a return to a more stratified water column with sea-ice loaded surface waters and still Atlantic-sourced subsurface waters. After 4.2 ka BP increased Polar Water at the surface of the East Greenland Current and reduction of the Return Atlantic Water at subsurface levels led to freshening and reduced stratification of the water column and (near) perennial sea-ice cover. The Neoglaciation started at 3.2 ka BP at our location, characterized by a strengthened East Greenland Current. Cold subsurface water conditions with possible sea-ice cover and minimum surface water productivity persisted here throughout the last ~3 kyr.

1 Introduction

The acceleration of climatic changes in the Arctic and Subarctic regions is particularly marked by the drastic reduction of summer sea-ice cover. According to model simulations, the Arctic Ocean may become seasonally ice-free as early as 2040-2050 (Stroeve et al., 2012). However, despite the extreme societal and environmental relevance of this sea-ice reduction, Holocene marine environments and corresponding natural sea-ice states around Greenland are still not well understood. The Northeast (NE) Greenland continental shelf is a particularly important region for studying and understanding the mechanisms that control sea-ice formation, melt and drift. It is the broadest shelf along the Greenland margin, extending more than 300 km from the coastline. To the west it reaches the East Greenland coastline with its major marine-terminating outlets of the Greenland Ice Sheet, while to the east it is bounded by the Fram Strait, which is the only deep passage between the Arctic Ocean and the rest of the world oceans. This shelf region is highly sensitive to climate and ocean variability because it underlies the East Greenland Current (EGC), which, through the western Fram Strait, is the main pathway of export of sea ice and cold water masses from the Arctic Ocean into the North Atlantic Ocean (Rudels and Quadfasel, 1991). The outflow of melt water/sea ice is a key factor that determines the North Atlantic freshwater budget, stratification and influences the deep-water formation. Moreover, waters on the NE Greenland

https://doi.org/10.5194/cp-2021-59
Preprint. Discussion started: 2 June 2021

Climate of the Past Discussions
Open Access
EGU

continental shelf play a major role in the stability of the glacier outlets of the Northeast Greenland ice stream (Wilson and Straneo, 2015; Schaffer et al, 2017).

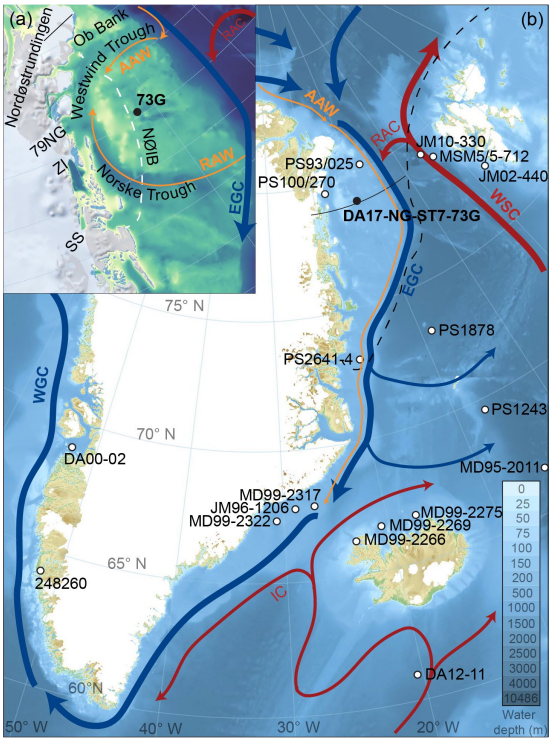

Figure 1(a): Close-up of the Northeast Greenland Shelf showing its characteristic features, the location of the studied sediment core (black circle) and the schematic subsurface circulation of the continental shelf (orange arrows). Arctic Atlantic Water (AAW), Return Atlantic Water (RAW), Nioghalvfjerdsfjorden Glacier (79NG), Zachariæ Isstrøm (ZI), Storstrømmen (SS), Norske Øer Ice Barrier (NØIB). (b): Overview map of the study area with the studied sediment core DA17-NG-ST07-73G (black circle; 'Rumohr core DA17-NG-ST07-72R was taken from the same site), other core sites mentioned in the text (open circles) and schematic illustration of the major currents. East Greenland Current (EGC), West Spitzbergen Current (WSC), Return Atlantic Current (RAC), Irminger Current (IC), West Greenland Current (WGC). Red arrows: warm surface currents, blue arrows: cold surface currents, orange arrow: cooled, Atlantic originated subsurface water mass, Arctic Atlantic Water (AAW). Core sites: PS93/025 (Syring et al., 2020a; Zehnich et al., 2020), PS100/270 (Syring et al., 2020b), JM10-330 (Consolaro et al., 2018), MSM5/5-712 (Müller et al., 2012; Werner et al., 2013), JM02-440 (Ślubowska-Woldengen et al., 2007), PS1878 (Telesinski et al., 2014a-b), PS2641-4 (Müller et al., 2012; Perner et al., 2015; Kolling et al., 2017), PS1243 (Bauch et al., 2001), DA00-02 (Seidenkrantz et al., 2008), MD99-2317 (Jennings et al., 2011), JM96-1206 (Jennings et al., 2002; Perner et al., 2016), MD99-2322 (Jennings et al., 2011), MD99-2275 (Ran et al., 2006), MD95-2011 (Giraudeau et al., 2010), MD99-2269 (Giraudeau et al., 2004, Giraudeau et al., 2010), MD99-2266 (Mooseen et al., 2015), 248260 (Seidenkrantz et al., 2007), DA12-11/2 (Van Nieuwenhove et al., 2018; Orme et al., 2018). Black line: location of the hydrographic transect pictured on Fig. 2b. Black dashed line: median sea-ice extent in September (1981-2010). The ocean bathymetry data are derived from GEBCO (Weatherall et al., 2015).

At the surface, the EGC carries cold and fresh polar waters southward. Below this low-salinity layer, the water column partly originates from submerged and recirculated Atlantic-sourced waters from the Arctic, and partly from the returning branch of the West Spitzbergen Current (Quadfasel et al., 1987) (Fig. 1). The EGC transports these water masses from the north into the Subpolar Gyre, then to the Labrador Sea and eventually, into the North Atlantic Ocean. The fresh water budget here is one of the major components that effects the strength of the Atlantic Meridional Overturning Circulation (AMOC; Rahmstorf, 1995; Clark et al., 2002). The AMOC is a main mechanism for the heat redistribution on our planet and acts as a control on the global climate. It transports warm and salty surface waters to high latitudes, where they cool, sink and return southwards at depth. Increased fresh water flux from the EGC to the North Atlantic may prevent deep convection, thus, reducing meridional heat transport, which causes

https://doi.org/10.5194/cp-2021-59
Preprint. Discussion started: 2 June 2021

Climate of the Past Discussions

cooling of the high latitudes (Clark et al., 2001). At present, due to the anthropogenic global warming, the AMOC may be in its weakest state in the last 1000 years (Caesar et al., 2021), urging an improved understanding of this complex system and its components.

The amount of polar waters transported northward in the EGC also depends on the North Atlantic Oscillation (NAO), one of the most prominent and recurrent patterns of atmospheric circulation variability. The NAO refers to a redistribution of atmospheric mass between the Arctic and the subtropical Atlantic, and its shifts from one phase to another produce large changes in the weather of the middle and high altitudes of the Northern Hemisphere (Hurrell et al., 2003).

Several studies suggest that the East Greenland shelf has been subjected to a series of oceanographic and paleoclimatic changes during the Holocene, induced by changes in the strength of the EGC linked to fluctuations in Atlantic Water entrainment. Most of these studies focus on the shelf region of Middle and South East Greenland (e.g., Jennings et al., 2002; Jennings et al., 2011; Müller et al., 2012; Perner et al, 2015; Perner et al., 2016; Kolling et al., 2017) and only few investigated the paleoceanographic evolution of the EGC in the northern part of the East Greenland shelf (Bauch et al., 2001; Syring et al., 2020a, 2020b; Zehnich et al., 2020). In this study, we aim to reconstruct the dynamics and variability of the EGC off NE Greenland at centennial resolution throughout the Holocene by micropaleontological, sedimentological and geochemical analysis of a sediment core retrieved from the central NE Greenland shelf. Faunal assemblage analysis of benthic and planktic foraminifera, stable isotope analysis, radiocarbon datings and X-ray fluorescence data allow us to infer changes in sea surface productivity, subsurface temperatures, sea-ice conditions and Greenland Ice Sheet melting over the last ca. 9.4 ka BP. The reconstruction provides new insights into the not yet resolved paleoceanographic evolution of this region, with comparisons to published records from the polar/subpolar North Atlantic.

2 Regional setting

The bathymetry of NE Greenland continental shelf is characterized by a trough system, consisting of five prominent cross-shelf troughs, which are deeper than the surrounding banks (Arndt et al., 2015). Nioghalvfjerdsfjorden Glacier (or 79 North Glacier, 79NG), Zachariæ Isstrøm (ZI) and Storstrømmen (Fig. 1) are the three major marine-terminating glaciers of the Northeast Greenland Ice Stream that drain in the area. Our study site is located approximately in the middle of the shelf in an inter-trough area between Westwind Trough and Norske Trough, facing the 79NG and ZI (Fig. 1). The location lies directly on the flow path of the EGC, as it flows southward along the Greenland shelf break (Johanessen, 1986), and over the middle to outer shelf (Bourke et al., 1987). Below a layer of local meltwater (Polar Surface Water, PSW), the upper part of the EGC carries cold, low saline (T: 0-1 °C, S<32) Polar Water (PW) from the Arctic Ocean in the upper ca. 250 m of the water column. At subsurface levels below the PW, the water mass has its origin from Atlantic-sources, to varying extent from the Return Atlantic Water (RAW; transported by the Return Atlantic Current, RAC) and from Arctic Atlantic Water (AAW; also sometimes named "Arctic Intermediate Water (AIW)") (Rudels et al., 2005) (Fig. 2). The RAC is the western branch of the West Spitzbergen Current that transports relatively warm and saline water masses (T<2 °C, S: 34-35) from the North Atlantic towards NE Greenland and southwards along the Greenland coast. In contrast, the eastern branch of the West Spitsbergen Current transports Atlantic Water (AW) into the Arctic Ocean, where it circulates at subsurface levels and cools. The AAW (T≥0 °C, S: 34-35) is formed by this recirculated cool AW, which again exits the Arctic Ocean and, together with the RAC, it forms the subsurface section of the EGC, as it flows southward along the East Greenland shelf (e.g., Quadfasel et al, 1987; Rudels, 2012). Along this southward path, the bathymetry on the NE Greenland shelf steers parts of the AW into the prominent cross-shelf troughs, toward the marine terminating glaciers of the Northeast Greenland Ice Stream, and thereby modulating the glaciers basal melt rates (Arndt et al., 2015; Schaffer et al., 2017).

https://doi.org/10.5194/cp-2021-59
Preprint. Discussion started: 2 June 2021

Climate of the Past Discussions
Open Access
EGU

The Polar Front in the Greenland Sea represents the eastern limit of perennial sea-ice cover, and the location of the sea-ice edge in the summer depends on the extent of the sea-ice export from the Arctic Ocean (Vinje, 1977). The sea-ice margin and the location of the Polar Front lies today east of our study site (Danish Meteorological Institute (DMI) and NSIDC, 2012), however, the Northeast Water (NEW) Polynya is in fairly close proximity to our core location. This is a seasonally ice-free or only loosely ice-covered area south of Nordøstrundingen (Fig. 1) on the eastern Greenland coast. Two ice barriers support the seasonal formation of the NEW Polynya, the Ob Ice Barrier by pushing drift ice eastward, while the Norske Øer Ice Barrier (NØIB) blocks the northward flowing sea ice which is entrained in the NE Greenland coastal current (Schneider and Budéus, 1994). It starts to open around May/June, then gradually increases its size and closes in September (Pedersen et al., 1993). The polynya's maximum extent to the north can reach high latitudes up to 83°N, beyond the NE Greenland shelf, and to the east the polynya can occupy the entire NE Greenland shelf with only little sea-ice left in the area (Schneider and Budéus, 1997).

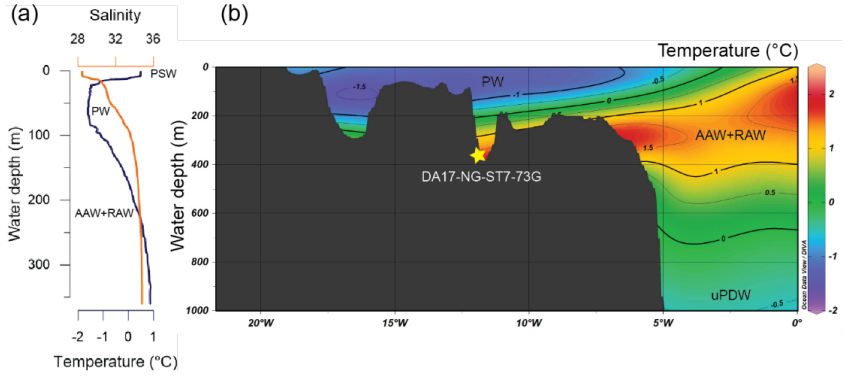

Figure 2(a): Temperature and salinity profile of the water column at the core site (79.073° N 11.918° W) obtained during the NorthGreen17 expedition, showing the main water masses. (b): Temperature of the water column in the upper 1000 m along a transect at 78.8755° N, showing the main water masses at the study site. Polar Surface Water (PSW), Polar Water (PW), combined Arctic Atlantic Water (AAW) and Return Atlantic Water (RAW), as well as upper Polar Deep Water (uPDW). The yellow star indicates the location of the core site at 385 m water depth. Temperature data from World Ocean Atlas 2018 (Boyer et al., 2018). The location of this transects is marked as a black line on Fig. 1b.

3 Material and methods

Gravity core DA17-NG-ST7-73G (79.068° N 11.903° W) was collected during the NorthGreen Expedition in September 2017 at 385 m water depth in an isolated bathymetrical depression on the NE Greenland shelf (Fig. 1). In addition, we collected Rumohr core DA17-NG-ST7-72R (79.072° N 11.888° W, 384.6 m water depth) with an intact sediment-water interface from the same station, which provided information for the age model of the gravity core. Temperature and salinity of the water column were measured in situ by a Seabird CTD (Conductivity-Temperature-Depth) profiler before the deployment of the gravity corer, with the core site being identified based on Innomar® subbottom profiler data obtained prior to coring.

The 410 cm long gravity core (73G) and the 88 cm long Rumohr core (72R) were stored at ca 3 °C before they were split lengthwise. The archive halves were scanned with an Itrax X-ray fluorescence core scanner (Cox Analytical) at the Department of Geoscience, Aarhus University (AU), Denmark. The scan was conducted with a Molybdenum tube (other settings: stepsize: 200 µm; exposure time: 10 s; voltage: 30 kV, current: 30 mA). The core scanning provided a line scan image, a 2-cm-wide radiographic image of the

https://doi.org/10.5194/cp-2021-59
Preprint. Discussion started: 2 June 2021


Climate of the Past Discussions

center of the core (voltage: 60 kV; current: 45 mA; exposure time: 2000 ms) and high-resolution analysis of bulk geochemical composition. From the results of the X-ray fluorescence scanning, we show the elements Si, K, Ti and the Ca/Fe ratio on Fig. 3.

The age-depth model of core 73G is based on six Accelerator Mass Spectrometry radiocarbon (AMS ^{14}C) dates, of which five are of mixed benthic foraminifera and one is of a worm tube lining. AMS ^{14}C dating was performed at the Laboratory of Ion Beam Physics, ETH Zürich, Switzerland. Radiocarbon ages were calibrated using the Marine20 calibration dataset (Heaton et al., 2020) and a local marine reservoir age correction (ΔR) of 0 ± 50 years (Reimer and Reimer, 2001). The age-depth model was made with the OxCal v4.4 software (Ramsey, 2008), using a P-sequence depositional model. Beyond the lowest radiocarbon date, the model is extrapolated toward the bottom of the core. The age of the upper part of the core is constrained by correlation to Rumohr core 72R by selected XRF elements (appendices, Fig. A1), to determine the amount of top sediment lost during gravity coring.

Samples for foraminiferal, ice-rafted debris (IRD) and stable isotope analyses were taken at 5 cm intervals at the Department of Geoscience, AU. The samples were weighed, wet-sieved with distilled water through sieves of 1000, 100 and 63 µm, dried at 40 °C for 24 hours and weighed again. For the foraminiferal assemblage analyses both planktic and benthic (calcareous and agglutinated) species were counted and identified to species level under a stereomicroscope for the size fractions of 63-100 µm and >100 µm; counts were subsequently combined prior to percentage calculations. When the samples contained excessive material, prior to counting they were split into equal parts containing >300 specimens, using a microsplitter. In these cases, foraminiferal tests of one part were counted and identified, and the total number of foraminifera was calculated. A minimum of 300 benthic specimens were identified for each sample, except for four samples (10-11 cm, 15-16 cm, 30-31 cm, 195-196 cm). These four samples contained only between 242-296 specimens. These data were, therefore, treated with some caution, but they were still included in the calculations for relative and absolute abundances. Absolute foraminiferal concentrations were calculated as individuals/g wet sediment. Relative abundances of both benthic agglutinated and calcareous species were calculated as a percentage of the total benthic (calcareous and agglutinated) foraminiferal fauna. However, diagrams of the separate percentage calculations of the two benthic foraminiferal groups (agglutinated species of total agglutinated assemblage and calcareous species of total calcareous assemblage) is shown in the appendices (Figs. A2 and A3).

For stable isotope analysis 5-200 specimens of the benthic foraminiferal species *Elphidium clavatum* were picked from every sample. The number of picked tests was restricted by the number of available, clearly identifiable tests. The specimens belonged mainly to the size 100-1000 µm fraction, supplemented with few specimens from the 63-100 µm fraction, when necessary. The oxygen and carbon isotope analysis of foraminiferal calcite was performed at the Leibniz Laboratory for Radiometric Dating and Stable Isotope Research at the Christian-Albrechts-University of Kiel using a MAT253 (Thermo Scientific) mass spectrometer system and a Kiel IV carbonate preparation device, with an analytical accuracy of <0.08 ‰ for $\delta^{18}O$ and <0.05 ‰ for $\delta^{13}C$. Results are expressed in δ notation referring to the PDB (Pee Dee Belmnite) standard, while using NBS-19 and IAEA-603 carbonate standards.

The content of IRD was calculated at 5 cm sample intervals using the dry weight of the size fraction >1000 µm divided by the wet weight of the whole sample.

Grain size distribution was measured on 42 samples (taken at 10-cm interval) by a laser particle sizer (Sympatec Helos) at the Department of Geoscience, AU, and grouped into three fractions: sand (>60 µm), silt (2-60 µm) and clay (<2 µm).

https://doi.org/10.5194/cp-2021-59
Preprint. Discussion started: 2 June 2021

Climate of the Past Discussions
Open Access
EGU

4 Results

4.1 Core description

Core DA17-NG-ST7-73G consist entirely of olive grey (5Y 4/1) marine silt with some clay, except the lowermost part of the core. The sediment of the lowest 40 cm of the core is much coarser, containing up to 51 % sand; it is also darker in colour (Fig. 3). In the rest of the core the sand fraction is on average 1.5 %.

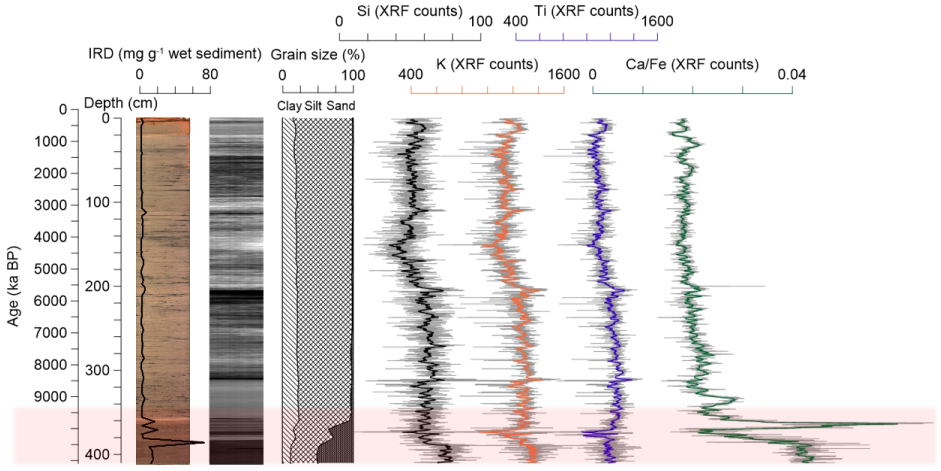

Figure 3: Results of the sedimentological and XRF core scanning analyses of core DA17-NG-ST7-73G. The bottom 65 cm of the sediment core is marked with rose-pink colour. The photograph and radiograph of the core were horizontally stretched.

4.2 Chronology

The age model was developed using six AMS ^{14}C measurements on mixed benthic foraminifera and on a worm tube lining from core 73G (Table 1). In order to evaluate potential loss of core top sediment during the coring process, we compared the XRF data of gravity core 73G and Rumohr core 72R (Fig. A1 in appendices), which indicated that 12 cm sediment was missing from the top of core 73G; this information was used when constructing the age model of core 73G. This age model suggest that the 410 cm long sediment core covers the last ~11.2 ka BP (Fig. 4). However, the results of the grain size, IRD and X-ray fluorescence analysis indicate that beyond the lowest radiocarbon date (at 345 cm depth, 9.4 ka BP) the sediments change significantly (Fig. 4). In the bottom 65 cm of the core preliminary analysis of foraminiferal content revealed the presence of species indicating a Pliocene or early Pleistocene age (Feyling-Hanssen, 1976; Feyling-Hanssen, 1980; Feyling-Hanssen et al., 1983), in addition to the normal in situ foraminiferal assemblage. We suggest that these Plio-/Pleistocene foraminifera are reworked into a glaciomarine setting. Due to this very different environment and the lack of ^{14}C dates in this interval, the age model of the bottom 65 cm of core 73G is currently uncertain. Therefore, apart from a short description of the foraminiferal content in the results, we have omitted the bottom 65 cm of the core (between 345 and 410 cm) from further analyses and discussion, focussing on the last 9.4 ka.

https://doi.org/10.5194/cp-2021-59
Preprint. Discussion started: 2 June 2021

Climate of the Past Discussions
Open Access
EGU

195 **Table 1: List of radiocarbon dates and modelled ages in core DA17-NG-ST7-73G. All dates were calibrated using the Marine20 calibration curve and ΔR=0 ± 50 years.**

Lab. ID	Depth (cm)	Material	Radiocarbon age (yr BP)	Error (yr)	Calibrated 2-sigma (BP)			Modelled 2-sigma (cal yr BP)		
					from	to	median	from	to	median
ETH-95387	70.5	Mixed benthic foraminifera	2475	60	2200	1705	1952	2161	1817	1989
ETH-95388	110.5	Mixed benthic foraminifera	3275	70	3190	2715	2935	3165	2783	2972
ETH-110893	226	Worm tube lining	5645	30	6029	5622	5835	6031	5678	5857
ETH-95389	250.5	Mixed benthic foraminifera	6015	70	6468	5994	6241	6643	6275	6458
ETH-95390	300.5	Mixed benthic foraminifera	7595	70	8097	7654	7870	8151	7761	7942
ETH-95391	345.5	Mixed benthic foraminifera	9015	70	9823	9295	9536	9602	9125	9383

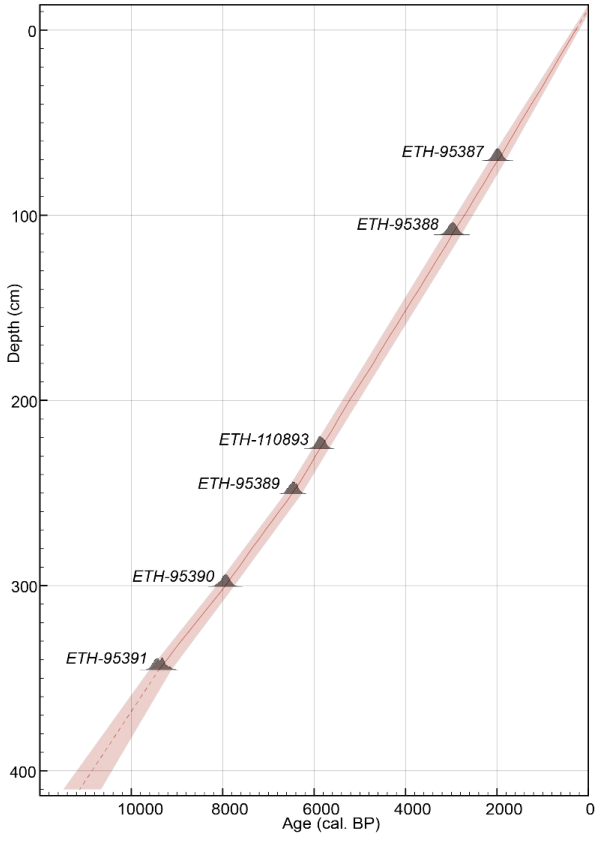

200 **Figure 4: Age-depth model of core DA17-NG-ST7-73G based on six AMS 14C dates and on the comparison with Rumohr core DA17-NG-ST7-72R. The shading in pink illustrates the 2-sigma uncertainty range of the model. The dotted line beyond the lowest radiocarbon date is extrapolated and highly uncertain.**

https://doi.org/10.5194/cp-2021-59
Preprint. Discussion started: 2 June 2021


Climate of the Past Discussions

4.3 X-ray fluorescence

Throughout the whole core, Si, K and Ti follow the same pattern. All three records show a relatively stable trend from the base of the core until ~318 cm depth (ca. 8.5 ka BP). At 316 cm (ca. 8.4 ka BP) all three elements displays peak counts, followed by a decrease until 161 cm (ca. 4.2 ka BP). There is a short-term drop in all three element counts at 161 cm depth (ca. 4.2 ka BP), which is followed by a steady increase until the top of the core (Fig. 3). The Ca/Fe ratio follows a steadily decreasing trend throughout the core, with slightly stronger fluctuations from the end of the core until ~270 cm (ca. 7 ka BP) and in the top 55 cm (last ~1.5 ka BP). The record shows a pronounced peak between 335 and 338 cm (ca. 9.1 ka BP), and two minor peaks at ~213 cm (ca. 5.5 ka BP) and at ~34 cm (ca. 0.9 ka BP) (Fig. 3).

4.4 Foraminiferal content

4.4.1 410-345 cm core depth

The bottom 65 cm of the core are characterised by a mixture of two assemblages. An assemblage of relatively small, well-preserved specimens of Arctic species include *Cassidulina reniforme, Elphidium clavatum, Islandiella norcrossi* and *Melonis barleeanum.* This assemblage is mixed with large specimens of *Cibicidoides grossus, Cibicides scaldiciensis, Islandiella inflata, Bulimina marginata, Cassidulina teretis, Elphidium funderi, Faujasina* sp., several of which are extinct since the early or mid Pleistocene (Feyling-Hanssen, 1976; Feyling-Hanssen, 1980; Feyling-Hanssen et al., 1983; Seidenkrantz, 1995), as well as some unusually large specimens of *E. clavatum, Haynesina orbiculare* and *Islandiella islandica*. This latter assemblage we interpret as reworked from older deposits.

4.4.2 345-0 cm core depth

We counted in total 70 samples, and identified 65 benthic (44 calcareous and 21 agglutinated) and three planktic foraminiferal species (Table A1 in the appendices) in the top 345 cm of core 73G. Both benthic and planktic specimens were well-preserved and showed minor or no signs of post-mortem dissolution of the tests.

The foraminiferal content is relatively low throughout the core, the benthic foraminiferal concentration varies between 17 and 158 individuals (ind.) g^{-1} wet sediment (sed.) (calcareous 2-128 ind. g^{-1} sed., agglutinated 10-55 ind./g sed.) (Fig. 5).

The concentration of planktic foraminifera is extremely low throughout the core, it lies between 0 and 13 ind. g^{-1} sed. Planktic foraminifera are represented primarily by the polar species *Neogloboquadrina pachyderma*, occasionally accompanied in the interval between 340-130 cm (ca. 9.4-3.4 ka BP) by specimens of the subpolar species *Turboratalita quinqueloba* and *Neogloboquadrina incompta*. The overall occurrence of planktic foraminifera is averaging 2 % of the total foraminiferal fauna.

On average, benthic agglutinated foraminifera account for 65 % of the total foraminiferal assemblage. From the end of the record until 210 cm (ca. 5.4 ka BP) the calcareous species periodically outnumber the agglutinated, however, from this point on and until the top of the record, agglutinated foraminifera continuously dominate the benthic assemblage (Fig. 5). Throughout the core, the most abundant benthic agglutinated species are *Portatrochammina bipolaris*, followed by *Ammoglobogerina globigeriniformis*, representing on average 42 % and 16 % (respectively) of the benthic agglutinated assemblage, and 27.5 % and 10.5 % of the total benthic assemblage. They are both continuously present throughout the core and their relative abundances do not show strong fluctuations (Fig. 6).

Benthic calcareous foraminifera represent on average 33 % of the total foraminiferal assemblage. The most abundant benthic calcareous species are *C. reniforme*, *E. clavatum*, *Cassidulina neoteretis* and *Stetsonia horvathi*. From these four species the

https://doi.org/10.5194/cp-2021-59
Preprint. Discussion started: 2 June 2021

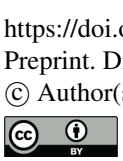

Climate of the Past Discussions
Open Access
EGU

abundances of *E. clavatum* shows the least variability throughout the record, however, it follows a steadily decreasing trend towards the top of the core (Fig. 5).

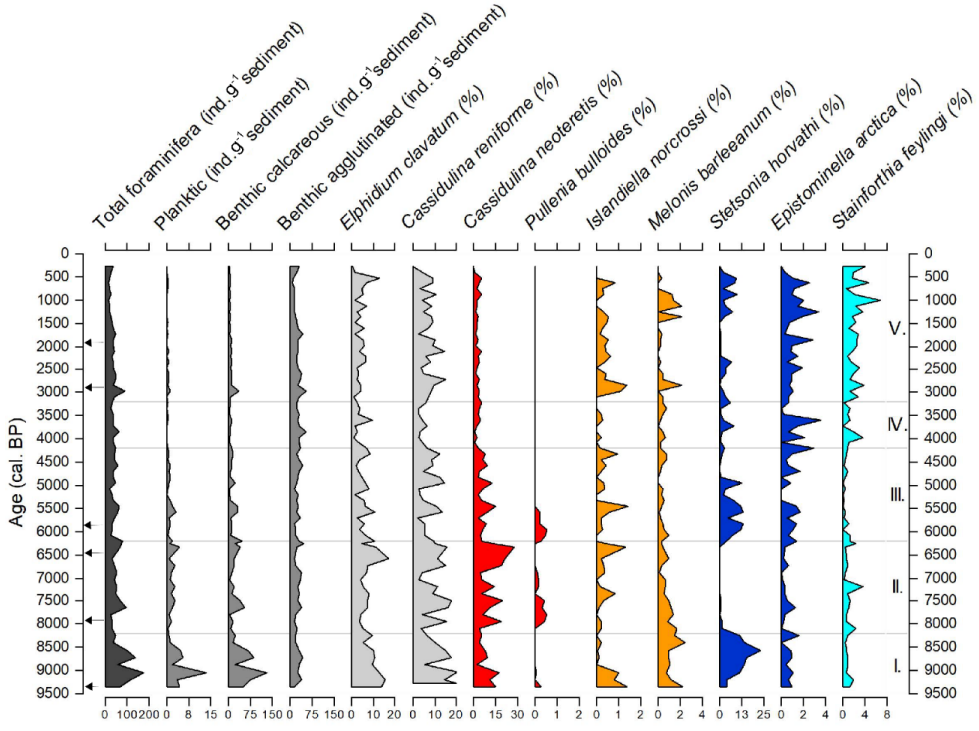

Figure 5: Foraminiferal concentrations and relative abundances of nine selected benthic calcareous species (expressed as a percentage of total benthic foraminiferal content) versus calibrated age along sediment core DA17-NG-ST7-73G. The depicted species were chosen in order to show changes in the environment. Red colour represents species that indicate warm Atlantic Water inflow; orange represents species that indicate in the Arctic recirculated, chilled Atlantic Water influence; dark blue represents Artic Water species; light blue represents a species that indicates sea ice. Ecozones (I.-V.) are shown on the right side of the figure. Black arrows next to the left y-axis mark radiocarbon dates. Note that the x-axes have different scaling.

In the following sections, we describe foraminiferal assemblage zones (ecozones) that were defined by visual interpretation of the species abundances. Boundaries were placed where major changes occurred in the relative abundances of the most abundant benthic calcareous and agglutinated species, indicating changes in the environment (Figs. 5 and 6).

4.4.3 Ecozone I. (345-310 cm; ca. 9.4-8.2 ka BP)

This ecozone is characterized by the highest content of total foraminifera (171 ind. g^{-1} sed.), including the highest concentrations of planktic (13 ind. g^{-1} sed.) and benthic calcareous (128 ind. g^{-1} sed.) foraminifera throughout the core. These three categories show two peaks in this interval: the first and bigger at ca. 9 ka BP and the second, smaller one at ca. 8.7 ka BP. We find in this interval the lowest agglutinated/calcareous ratio, as the calcareous specimens almost continuously outnumber the agglutinated ones. The average concentration of agglutinated foraminifera is 29 ind. g^{-1} sed. in this zone, and it does not vary significantly throughout the other intervals either (27-29 ind. g^{-1} sed.). The benthic calcareous assemblage is dominated by *C. reniforme* (relative abundance on average 14 %), followed by *S. horvathi* (on average 12 %), *E. clavatum* (on average 11 %) and *C. neoteretis* (on average 9 %).

https://doi.org/10.5194/cp-2021-59
Preprint. Discussion started: 2 June 2021

Climate of the Past Discussions
Open Access
EGU

4.4.4 Ecozone II. (310-245 cm; ca. 8.2-6.2 ka BP)

In this ecozone, we can recognize a distinctive decrease in planktic and benthic calcareous foraminiferal concentrations, and as a consequence, a higher benthic agglutinated/calcareous species ratio. The relative abundance of *C. neoteretis* promptly increases, and it becomes the dominating species of the benthic calcareous fauna in this interval (highest relative abundance 27 %, on average 13 %), followed by *C. reniforme* (on average 10 %). *Pullenia bulloides* suddenly appears in the record and, at the same time, the relative abundance *S. horvathi* drastically decreases and it remains around 1 % during the whole period. Even though the relative abundances of *E. clavatum* decrease compared to the previous interval, this species shows its highest relative abundance throughout the core in this ecozone at 255 cm (17 %; ca. 6.5 ka BP).The relative abundance of agglutinated species *Adercotryma glomerata* significantly increases from 310 cm on and remains on the same level throughout this zone.

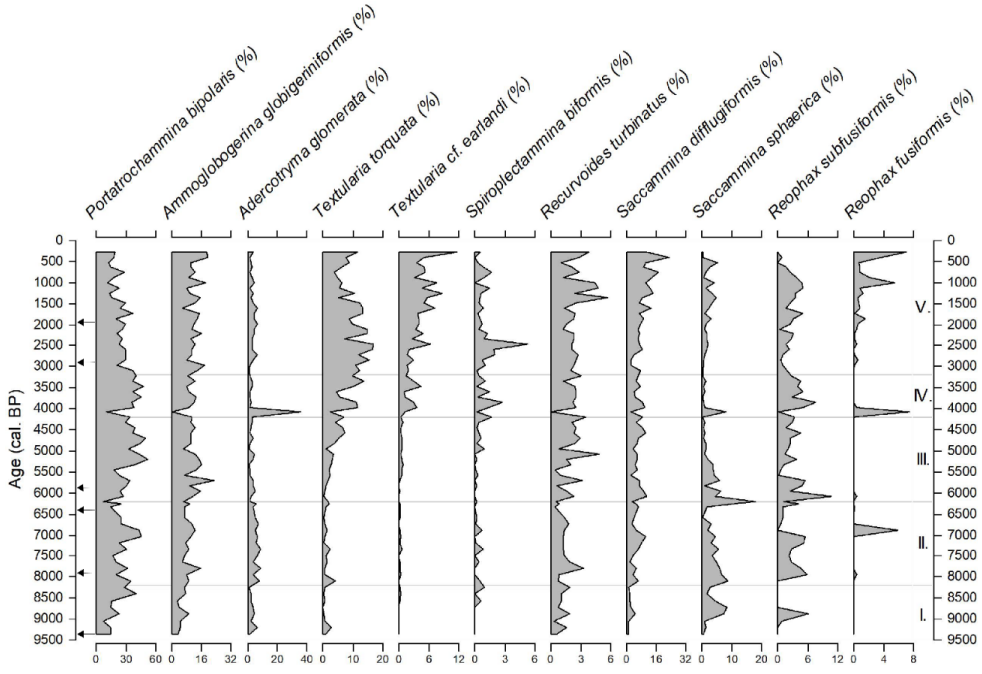

Figure 6: Relative abundances of the most abundant (>5% in at least one sample) benthic agglutinated foraminifera species (expressed as a percentage of total benthic foraminiferal content) versus calibrated age along sediment core DA17-NG-ST7-73G. Ecozones (I.-V.) are shown on the right side of the figure. Black arrows next to the left y-axis mark radiocarbon dates. Note that the x-axes have different scaling.

4.4.5 Ecozone III. (245-165 cm; ca. 6.2-4.2 ka BP)

The concentrations of planktic and benthic calcareous foraminifera continue to decrease in this ecozone. From 245 cm, the relative abundance of *C. neoteretis* drops back to 7 % (on average), while the relative abundance of *S. horvathi* rises dramatically (from 1 % to 7 %). *Epistominella arctica* also increases (from 0.4 % (previous interval) to 0.8 %), just like *Textularia torquata*, while the relative abundances of *A. glomerata* decreases.

4.4.6 Ecozone IV. (165-125 cm; ca. 4.2-3.2 ka BP)

The base of this ecozone is defined by the drastic decrease in benthic calcareous foraminifera concentrations (from 15.7 to 8.4 ind. g^{-1} sed.), and increased relative abundances of *E. arctica* and *Stainforthia feylingi*. *C. neoteretis* drops dramatically (to 3 % on average), just like *C. reniforme* that reaches its lowest relative abundance in this zone (on average 5 %). On the other hand,

https://doi.org/10.5194/cp-2021-59
Preprint. Discussion started: 2 June 2021

Climate of the Past Discussions

agglutinated species *A. glomerata* shows a drastic peak at the beginning of this ecozone, and the relative abundances of *T. torquata*, *Textularia* cf. *earlandi* and *Spiroplectammina biformis* increase significantly compared to the previous interval.

4.4.7 Ecozone V. (125-0 cm; ca. 3.2-0.3 ka BP)

The concentrations of planktic foraminifera and the relative abundances of *C. neoteretis* further decrease and reach their lowest level throughout the core, while *C. reniforme* shows an increase compared to ecozone IV, just like *S. feylingi*. The relative abundances of agglutinated species *T. torquata*, *T.* cf. *earlandi* and *S. biformis* continue to increase, while *Saccamina difflugiformis* shows a steep rise unique to this interval.

4.5 Stable isotopes

From the 70 analysed samples the results of three samples were not accepted: one (180 cm) due to technical problems, and two gave too low signal due to small sample size (0 cm and 130 cm). The sample at 140 cm gave a comparatively very low $\delta^{18}O$ (2.25 ‰) and a very high $\delta^{13}C$ value (-1.07 ‰), but these outliers were nonetheless accepted.

Except for the one outlier, the variation of $\delta^{18}O$ values is rather small throughout the core (between 2.85 and 3.69 ‰, with a mean of 3.29 ‰), and the values show a stable trend, albeit with a slight increase towards the top of the core. The $\delta^{13}C$ values show a constant increase from the bottom to the top of the core, varying between -1.07 and -2.61 ‰ (Fig. 7).

5 Environmental significance of foraminiferal assemblages

In order to be able to describe the changes in water masses over time on the NE Greenland shelf, we place selected benthic calcareous foraminifera species into groupings that are based on environmental preferences of the species (Table A2 in appendices). The Atlantic Water group includes *C. neoteretis* and *P. bulloides*. These species indicate warm and saline AW inflow underneath cold and low salinity surface waters (e.g., Mackensen and Hald, 1988; Seidenkrantz 1995; Rytter et al., 2002; Jennings et al., 2004; Jennings et al., 2011; Cage et al., 2021). The chilled Atlantic Water group includes *I. norcrossi* and *M. barleeanum*. These species have been previously linked to cool AW (e.g., Slubowska-Woldengen et al., 2007; Perner et al., 2011; Perner et al., 2015; Cage et al., 2021), and we use them to represent the relative contribution of chilled AW recirculated in the Arctic Ocean to the EGC. The Arctic Water group includes *S. horvathi* and *E. arctica*. Both species live at present beneath perennial sea ice, in the deeper part of the Arctic Ocean, thus indicating cold, Arctic originated deep-waters (e.g., Green, 1960; Lagoe, 1979; Wollenburg and Mackensen, 1998; Jennings et al, 2020). We consider *S. feylingi* as a sea-ice edge indicator species that tolerates unstable conditions (Knudsen and Seidenkrantz, 1994; Seidenkrantz, 2013); its increase may refer to the location of a sea-ice margin at the study site. Moreover, we use in the interpretation the abundances of the agglutinated species *A. glomerata*, *T. earlandi*, *T. torquata*, *S. biformis* and *S. difflugiformis*. *A. glomerata* is often correlated with Atlantic sourced waters in high latitudes (e.g., Hald and Korsun, 1997, Lloyd 2006; Perner et al., 2012). Many studies find *T. earlandi*, *T. torquata* and *S. biformis* in areas influenced by cold, low-salinity Arctic water, often in glaciomarine environments (e.g., Jennings and Helgadottir, 1994; Korsun and Hald, 2000; Perner et al, 2012; Perner et al., 2015, Wangner et al., 2018). *S. difflugiformis* is described as closely associated with Polar Water on the East Greenland shelf and fjords (Jennings and Helgadottir, 1994).

https://doi.org/10.5194/cp-2021-59
Preprint. Discussion started: 2 June 2021

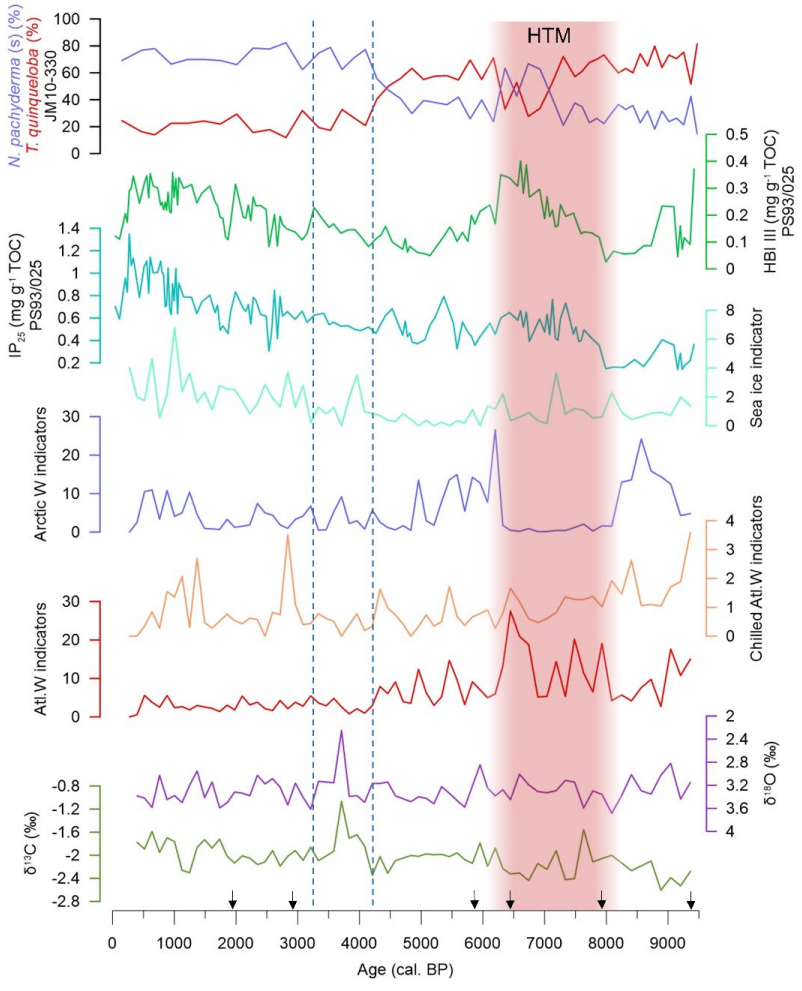

315 **Figure 7: From the bottom to the top: $\delta^{18}O$ and $\delta^{13}C$ results and relative abundances of the four benthic calcareous foraminifera groupings (based on environmental preferences of the contained species, see Fig. 5 and Appendix Table A1) from this study (core 73G), compared to other proxy records from the NE Greenland shelf and western Svalbard. HBI III and IP_{25} from core PS93/025 (Syring et al., 2020a). Relative abundances of planktic polar species *Neogloboquadrina pachyderma* (sin.) and subpolar species *Turborotalita quinqueloba* from core JM10-330 (Consolaro et al., 2018). HTM: Holocene Thermal Maximum. Black arrows on the x-axis mark**
320 **radiocarbon dates.**

6 Discussion

6.1 Origin of Atlantic-sourced water at the core site

Although the study site is located on the central flow route of the EGC, the path of the influx of the Atlantic-sourced water, which is clearly identified as the bottom layer through the CTD (Fig. 2), is less clear. The temperature profile with bottom water
325 temperatures not exceeding 1 °C suggest that the Atlantic-sourced water is closer in character to that found in Westwind Trough

https://doi.org/10.5194/cp-2021-59
Preprint. Discussion started: 2 June 2021


Climate of the Past Discussions

than the Atlantic-sourced water presently seen in Norske Trough. This may indicate a primarily AAW source (Rudels et al., 2005; Schaffer et al., 2017). The Atlantic-sourced water may thus reach the site via the Westwind Trough, but may also be due to wind-driven upwelling. This process leads to considerable modification of local water masses and shelfbreak exchanges (e.g., Estrade et al., 2008). In the Arctic it is often associated with the onshore transport of warm, and relatively salty AW to the continental shelves (e.g., Kirillov et al., 2016).

6.2 Paleoenvironmental interpretation

6.2.1 Bottom 65 cm of the sediment core

The combined presence of an assemblage of well-preserved small tests of Arctic foraminiferal species and many extinct Plio-Pleistocene specimens suggest that a Plio-Pleistocene assemblage was reworked from older deposits such as Kap København (Feyling-Hanssen, 1976; Feyling-Hanssen, 1980; Feyling-Hanssen et al., 1983; Funder et al., 2001), into a glaciomarine environment with in situ Arctic foraminifera. Potentially the breakup and significant retreat of a nearby glacier caused reworking of older sediments as also previously suggested for other sites (e.g., Seidenkrantz et al., 2019), but further studies are required to resolve this issue.

6.2.2 Early Holocene (ca. 9.4-8.2 ka BP; ecozone I.)

This cold interval was characterized by high percentages of *S. horvathi*, which has previously been considered linked to high sea-ice concentrations (e.g., Green, 1960; Lagoe, 1979; Wollenburg and Mackensen, 1988; Jennings et al., 2020) combined with the presence of Atlantic Water indicator species. This combination of Atlantic-sourced bottom water and sea ice points to a highly stratified water column in the early Holocene (Fig. 5). Cold, heavily sea ice-loaded surface waters entrained in PW of the upper EGC would have characterised the upper water column, while at the same time the influx of warm Atlantic-sourced water from either the RAC or the AAW (or a combination of both) was also strong. When compared to the data from the top of the core, the water column stratification between the cold and warmer waters was likely more pronounced than today. Relatively high counts of the terrestrially-derived elements Si, K and Ti, together with relatively low $\delta^{18}O$ values indicate increased meltwater influence from the Greenland Ice Sheet (Figs. 3 and 7).

The interval was also characterised by high surface water productivity, as shown by high concentrations of planktic and benthic calcareous foraminifera, the presence of *E. arctica*, which thrives in high-productivity environments (Wollenburg and Kuhnt, 2000) and a pronounced peak in Ca/Fe ratio, which is considered as a general proxy for paleoproductivity (e.g., Vare et al., 2009). The planktic foraminifera may have been transported to the site in the subsurface water layer from a nearby more open-ocean site, but they still suggest increased surface water-bioproductivity in the general region. Low and slowly rising benthic $\delta^{13}C$ values can also be related to high level of bioproductivity, due to decomposition of isotopically light organic carbon in the lower part of the water column. We propose that high productivity combined with sea-ice indicates that our site was located west of the Polar Front, but that the Polar Front was situated in close proximity to our location in this time interval. It should be noted that in the XRF data, we recognize a short-lived, but clear peak in terrestrially-derived sediments around 8.5-8.4 ka BP (Fig. 3). This may be potentially linked to increased iceberg release during the so-called 8.2. ka event (i.a., Alley et al., 1997; Barber et al., 1999), however, this signal seems to be only reflected in the results of the sedimentological analyses, and not in the foraminiferal assemblage changes/stable isotope results, although the lower temporal resolution of the latter may also not allow us to identify any changes.

Our suggestions of cold water and sea ice at the surface is in accordance with a recent sea-ice reconstruction from the NE Greenland shelf (Syring et al., 2020a; core PS93/025). That study reveals a cold interval with increased sea-ice cover between 9.3 and 7.9 ka

https://doi.org/10.5194/cp-2021-59
Preprint. Discussion started: 2 June 2021


Climate of the Past Discussions

BP, shown by lower concentrations of marginal sea-ice proxy HBI III and IP_{25}, interpreted as low sea-ice algal productivity caused by an expansion of the sea-ice cover (Fig. 7). Foraminiferal records from the Southeast Greenland shelf (Jennings et al., 2011; cores MD99-2322 and MD992317) suggests similarly cold and unstable sea-surface conditions between 9.4 and 8.1 ka BP. Moreover, cool deep-water conditions in the eastern Fram Strait during this period (Consolaro et al., 2018; core JM10-330) point to a weakened RAC, suggesting that the strong water column stratification on the NE Greenland shelf was due to increased AAW influx.

6.2.3 Holocene Thermal Maximum (ca. 8.2-6.2 ka BP; ecozone II.)

The interval from 8.2 to 6.2 ka BP was characterised by the warmest bottom-water conditions of the Holocene on the NE Greenland shelf, as well as reduced sea-ice cover, as indicated by the almost complete absence of sea-ice indicator species and maximum abundances of Atlantic Water species and other species indicating stable bottom waters. *C. neoteretis* and *A. glomerata* had their highest relative abundances during this interval (except for an extreme peak of *A. glomerata* at ~4 ka BP), and *P. bulloides* appeared in the record after a long absence around 8 ka BP (Figs. 5 and 6), suggesting highly stable bottom waters (Rytter et al., 2002). A concurrent significant decrease in planktic and benthic calcareous foraminiferal concentrations indicates a transition towards lower surface and subsurface water productivity, also shown in decreasing Ca/Fe element ratios.

We suggest that this may be explained by a strengthening of the RAC, transporting RAW to our site and causing increased entrainment of warm Atlantic-sourced water into the EGC. As a consequence of likely vertical expansion of the Atlantic-sourced water layer, surface waters likely also warmed, and the Polar Front moved from our location to further north or further inland during this period, which represents the warmest of our record, and which we here refer to as the Holocene Thermal Maximum (HTM).

In the eastern Fram Strait several studies (Slubowska-Woldengen et al., 2007; core JM02-440; Müller et al., 2012; core MSM5/5-712; Consolaro et al., 2018; core JM10-330, see Fig. 1) recorded strong AW flow and warm sea-surface conditions until 7-6.8 ka BP (Fig. 7), which would have resulted in a stronger RAC. In line with our findings, Müller et al. (2012) (core PS2641-4) and Jennings et al. (2011) (cores MD99-2322 and MD99-2317) reconstructed relatively warm conditions during the first part of the mid Holocene on the ME and SE Greenland shelf in surface and subsurface waters, respectively. Also further south in the Nordic Seas, thermal optimum-like conditions with warm sea surface temperatures prevailed until ca. 6 ka BP (Bauch et al., 2001; core PS1243).

6.2.4 Cooling after the HTM (ca. 6.2-4.2 ka BP; ecozone III.)

From 6.2-4.2 ka BP benthic foraminiferal assemblages again start to resemble those of the period prior to 8.2 ka BP, with increased percentage of *S. horvarthi* and a decrease in the Atlantic water indicator *C. neoteretis* (Fig. 5). This suggests return to a more stratified water column with sea-ice loaded surface water and Atlantic-sourced subsurface waters. However, in contrast to Ecozone I, neither the benthic and planktic foraminiferal concentrations nor stable isotope data suggest increased bioproductivity.

Along West Spitzbergen the inflow of subsurface AW, and thus the RAC weakened after 7 ka BP (Consolaro et al., 2018; core JM10-330;), and a gradual cooling of surface waters started around 7-6.6 ka BP (Müller et al., 2012; core MSM5/5-712), accompanied by increased sea-ice cover (Slubowska-Woldengen et al., 2007; core JM02-440). A sediment core retrieved north from our location (Syring et al., 2020a; Zehnich et al., 2020; core PS93/025) shows seasonally more extended sea-ice cover (derived from decreasing HBI III and increasing IP_{25} concentrations; Fig. 7) and decreasing primary production after 5.5 ka BP.

https://doi.org/10.5194/cp-2021-59
Preprint. Discussion started: 2 June 2021


Climate of the Past Discussions

Accordingly, at the same time, Perner et al. (2015) (core PS641-4) recorded the southward relocation of Polar Front to close to their site in the Foster Bugt area. Giraudeau et al. (2004) (core MD99-2269) and Ran et al. (2006) (core MD99-2275) recorded increased influence of cool, low salinity polar waters of the EGC on the North Iceland Shelf between 6.5-3.5 ka BP and 6.8-5.6 ka BP, respectively. In the Iceland Basin a long- term cooling trend started at between 6.8 and 6.1 ka BP (Orme et al., 2018; Van Nieuwenhove et al., 2018; core DA12-11/2).

6.2.5 Further cooling in the mid Holocene (ca. 4.2-3.2 ka BP; ecozone IV.)

Our record shows clear evidence for significant changes occurring at 4.2 ka BP. The period starts at our location with a sudden rise in the relative abundances of calcareous sea-ice indicator species *S. feylingi* and in the relative abundances of agglutinated species *T. earlandi*, *T. torquata* and *S. biformis* (Figs. 5 and 6), which are often connected to cold, low-salinity PW (Jennings and Helgadottir, 1994; Korsun and Hald, 2000; Perner et al., 2012; Perner et al., 2015; Wangner et al., 2018). Furthermore, the interval is marked by lowest abundances of warm Atlantic Water species and very low concentrations (under 1 ind./g) of planktic foraminifera. The benthic agglutinated/calcareous foraminiferal ratio increases and the terrestrially derived elements Si, K and Ti show minimal values (Fig. 3), indicating very low meltwater influence in the EGC. Slightly higher benthic $\delta^{18}O$ values and increasing $\delta^{13}C$ values after 4.2 ka BP (Fig. 7) point also to general cooling and weak influence of AW. Accordingly, the light $\delta^{18}O$ spike found in the middle of this interval cannot be attributed to sudden bottom water warming on the basis of the foraminiferal fauna. It is more readily explained by brine rejection during sea ice formation, which can carry the light isotopic signal from the surface to the ocean bottom. It should here be noted that apart from a single sample with increased relative frequencies of the warmer-water agglutinated species *A. glomerata* (Figs. 6 and A3), there is no evidence of a shorter-lived climate excursion that might be linked to the so-called 4.2ka BP event (Weiss, 2017), only a general change in environment at this time.

We suggest that increased PW at the surface of the EGC and reduction of the RAC at subsurface levels led to freshening and reduced stratification of the water column at our site; it may also have experienced (near) perennial sea-ice cover. The reduced strength of the RAC was likely caused by an overall decrease in AW transport from the south with the North Atlantic and West Spitsbergen currents to the eastern Fram Strait, accompanied by surface-water cooling and increased sea-ice coverage after 5.5 ka BP (Hald et al., 2007; core MSM5/5-712; Werner et al., 2013; core PS1878; Telesinski et al., 2014b; core PS1878; Consolaro et al., 2018; core JM10-330; Fig. 7). Harsh conditions and strengthened EGC with permanent sea-ice cover dominated the central Greenland shelf as well (Perner et al., 2015; Kolling et al., 2017; core PS641-4). Further south on the shelf Jennings et al. (2002) and Perner et al. (2016) (core JM96-1206) described increased PW influence in the EGC, glacier advance and iceberg rafting during this period.

6.2.6 Neoglaciation (ca. 3.2-0.3 ka BP; ecozone V.)

The period from ca. 3.2 – 0.3 ka BP is characterised by a further increase in the relative abundances of sea-ice edge indicator species *S. feylingi* and the agglutinated species *S. difflugiformis*. Atlantic-water indicator *C. neoteretis* is only found in relatively low numbers, although there is some increase in species linked to chilled Atlantic Water (Figs. 5, 6 and 7). Continuously increasing benthic $\delta^{13}C$ values indicate strong ventilation of the water column (Fig. 7). The results point to cold and unstable conditions with minimum surface water productivity and increasing sea-ice cover at our location. During this period, the EGC was likely strengthened compared to previously, with a thick layer of cold and fresh PW on the surface and recirculated AAW inflow from the Arctic at subsurface levels, as seen in the chilled Atlantic Water group.

https://doi.org/10.5194/cp-2021-59
Preprint. Discussion started: 2 June 2021


Climate of the Past Discussions

Previous studies have indicated that during the late Holocene, the WSC transported less and less heat (Slubowska-Woldengen et al., 2007; core JM02-440), causing less warm water to reach the EGC through the RAC. From West Spitzbergen (Müller et al., 2012; core MSM5/5-712; Consolaro et al., 2018; core JM10-330) and from several other locations in the Greenland Sea (e.g., Telesinski et al., 2014b, core PS1878) and West Greenland (e.g., Seidenkrantz et al., 2007; core 248260; Seidenkrantz et al., 2008; cores DA00-02P and DA00-03P) a general cooling trend has been reported, with more severe sea-ice conditions. On the Iceland shelf strongly reduced Irminger surface water and low coccolith carbonate sedimentation indicate extreme advection of polar waters and extended sea-ice development (Giraudeau et al., 2004; core MD99-2269).

6.3 Development of Holocene oceanographic conditions on the NE Greenland shelf

Early Holocene warming of the circum-Arctic region (Kaufmann et al., 2004) led to enhanced Greenland Ice Sheet and glacier melting around the Arctic. During the Last Glacial Maximum (~26-19 ka BP) the Greenland Ice Sheet extended onto the shelf offshore NE Greenland, perhaps even reaching the shelf break (Bennike and Weidick, 2001; Arndt et al., 2017). However, as a consequence of rising air temperatures due to the orbitally-forced Northern Hemisphere summer insolation maximum (reported at approximately 10 ka BP; Andersen et al., 2004; Jansen et al., 2008), the deglaciation of the outer coast and retreat of the ice margin to its present location occurred already between 11.7 and 9.3 ka BP (Larsen et al., 2018); the ice shelf of 79NG rapidly retreated through the fjord between 9.6 and 7.5 ka BP (Syring et al., 2020b). The drastic ice recession of the early Holocene produced an extended meltwater surface layer in the Greenland region prior to 8.6 ka BP (Seidenkrantz et al., 2013). The extensive melting of the Greenland Ice Sheet was strong enough to act as negative feedback to the early Holocene warming, and delayed the HTM with 2 kyr at our location compared to the eastern parts of the Nordic Seas (Blaschek and Renssen, 2013). Thus, between 9.4 and 8.2 ka BP cold, heavily sea ice-loaded surface waters and strongly stratified water column characterized the NE Greenland shelf. The strong freshwater discharge might have also have weakened the recording of the 8.2 ka cooling event at our location, although a short-term increase in terrestrial deposits suggest transport of sediments from land via meltwater or icebergs during this event. This cold event was described in a number of paleoceanographic archives from Greenland and the northern North Atlantic (e.g., Risebrobakken et al., 2003; Ellison et al., 2006; Rasmussen et al., 2007), and it is believed to be connected to the collapse of the Laurentide Ice Sheet and drainage of Lake Agassiz (e.g., Alley et al., 1997; Barber et al., 1999; Hillaire-Marcel et al., 2007; Hoffman et al., 2012). However, in many other records from areas that are mainly influenced by the EGC, WGC or the Baffin-Labrador Current system (Keigwin et al, 2005; Sachs 2007; Seidenkrantz et al., 2013), the 8.2 ka cooling event cannot be recognised; these sites were all characterised by the permanent presence of a low-salinity, cold surface layer at that time, which may also explain the weak signal of this event at our site.

After ca. 8.2 ka BP, our data suggest that increased entrainment of warm Atlantic-sourced water within the RAC changed the water column properties on the NE Greenland shelf. During the subsequent Holocene Thermal Maximum, both subsurface and surface water temperatures increased, and consequently, open water conditions prevailed in the next ca. 2 kyr close to our location. Due to the warming, the floating ice margin of 79NG decreased (Bennike and Weidick, 2001), but on the other hand, the fresh, less dense basal melt water of the glacier isolated the landfast sea-ice cover from the warm subsurface waters, and thus, stabilized the NØIB (Mayer et al., 2000; Syring et al., 2001b). Further south, parallel to the warming of the EGC (Jennings et al., 2011; Müller et al., 2012), the Irminger Current increased its strength, as recorded on the North Icelandic Shelf (Ran et al., 2006; Cabedo-Sanz et al., 2016).

https://doi.org/10.5194/cp-2021-59
Preprint. Discussion started: 2 June 2021


Climate of the Past Discussions

After the Thermal Maximum, cooling started on the NE Greenland shelf between 6.2 and 4.2 ka BP (e.g., this study; Andrews et al., 1997; Jennings et al., 2002; Zehnich et al., 2020), with decreased, but still persistent inflow of subsurface AW from the RAC. The EGC became stronger, with sea-ice loaded surface waters and relatively warm Atlantic-sourced subsurface waters. Coincident with the expansion of the EGC, several studies from the Nordic Seas (e.g., Bauch et al., 2001; Hall et al., 2004; Hald et al., 2007) infer a weakening of the AMOC, increased water column stratification and less ventilated subsurface during this period. In line with a decreased flux of recirculating AW onto the NE Greenland shelf, the Northeast Greenland Ice Margin started to advance from its mid Holocene minimum around 6 ka BP (Larsen et al., 2018). Reduced amounts of warm AW on the inner continental shelf most probably reduced the basal melting within the 79NG fjord and may have contributed to the re-advance of the ice shelf of 79NG seen from around 4.5 ka BP on (Bennike and Weidick, 2001; Syring et al., 2020b).

The Neoglacial cold interval started on the East Greenland shelf approx. 3.5-3.2 ka BP, with increased freshwater forcing from the Arctic Ocean and advance of the Greenland Ice Sheet (this study; Andersen et al., 2004; Jennings et al., 2011). According to model simulations of Renssen et al. (2006), the expansion of sea ice may be associated with a cooling triggered by a negative solar irradiance anomaly, which was amplified through a positive oceanic feedback mechanism. The cooling caused temporary relocation of deep-water formation sites in the Nordic Seas, which was accompanied by a distinct reduction in AMOC strength (Hall et al., 2004). The increase in sea-ice extent stratified the water column and hampered the deep-water formation, leading to additional cooling and more sea ice (Renssen et al., 2006).

6.4 Variations of AW and PW entrainment in the EGC during the Holocene and their implications for the general climatic trends in the Nordic Seas

Distinct variability in subsurface water mass properties on the NE Greenland shelf through the Holocene point to broad scale changes in the proportion of RAW/AAW and PW in the EGC, and thus, to a strong covariance with the northward heat transport in the Nordic Seas. The increased entrainment of warm Atlantic-sourced water into the EGC that we document during the HTM, coincides with increased advection of warm AW in the West Spitzbergen Current, driven by increased wind force and/or by stronger thermohaline circulation (Sarthein et al., 2003; Slubowska-Woldengen et al., 2007; Knudsen et al., 2011).

During the mid Holocene, the summer insolation declined at the northern latitudes due to the changes in the Earth´s orbital parameter (Berger, 1978). From 7 ka BP, the summer sea surface temperatures of the Nordic Seas started to decrease (Koç et al., 1993; Andersen et al., 2004). This cooled AW progressed northward carrying less and less heat to the North Atlantic and West Spitsbergen currents (Sarthein et al., 2003; Slubowska-Woldengen et al., 2007; Risebrobakken et al., 2011; Consolaro et al., 2018; Hald et al., 2007), also due to a weakened AMOC (e.g., Bauch et al., 2001; Hall et al., 2004; Hald et al., 2007; Knudsen et al., 2011). In response to the reduced warm water transport through the RAC, the proportion of cooled AW and PW in the EGC increased, which ended the ameliorated conditions on the East Greenland shelf.

The northward flow of AW with the North Atlantic and West Spitsbergen currents to the eastern Fram Strait, and consequently the RAW reaching the EGC, arrived to a minimum during the late Holocene, after 4.5 ka BP (Slubowska-Woldengen et al., 2007). Consequently, the EGC strengthened, carrying a thick layer of fresh PW southward. A pronounced colder period after 4 ka BP is recognized in some (but not all) reconstructions north and south of Iceland, in the Greenland Sea and to the west of Svalbard (Moossen et al., 2015; Orme et al., 2018; Telesinski et al., 2014b; Werner et al., 2016; respectively); in particular at locations influenced by the EGC. This gradual cooling trend in the northern North Atlantic is associated therefore with a continuous transition from a positive towards a negative NAO phase (e.g., Andersen et al., 2004; Orme et al., 2018). Positive NAO phases are

https://doi.org/10.5194/cp-2021-59
Preprint. Discussion started: 2 June 2021

accompanied by stronger westerlies carrying moist air over Europe and Siberia, an increased AW inflow through Fram Strait, and warmer temperatures in the Arctic, which lead to a reduction in sea-ice formation. During intervals of a negative NAO these phenomena are reversed (Kwok, 2000; Hurrell and Deser, 2010), and high pressure over Greenland and consequently strengthened northerly winds over East Greenland can lead to strengthened EGC and increased PW transport (e.g., Ionita et al, 2016). The late-Holocene trend towards a stronger and fresher EGC is likely to have increasingly impacted the Subpolar Gyre dynamics. Increased freshwater input to the Labrador Sea may have weakened the Subpolar Gyre circulation by preventing deep convection (Hillarie-Marcel et al., 2001), and consequently reduced the amount of water entrained into the North Atlantic Current (Moros et al., 2012). This, on the other hand, may have forced enhanced northward heat transport via the North Atlantic Current, and may have helped to restart (Thornalley et al., 2009) the previously weakened AMOC (e.g., Cronin et al., 2003; Oppo et al., 2003).

7 Conclusions

The presented multiproxy study, based on benthic foraminiferal assemblage-, geochemical- and sedimentological analyses of sediment core DA17-NG-ST7-73G allowed us to reconstruct changes in sea surface productivity, subsurface water temperatures, sea-ice conditions, Greenland Ice Sheet melting and thus, in the strength of the EGC over the last ca. 9.4 ka BP on the NE Greenland shelf.

- Between 9.4 and 8.2 ka BP the water column was highly stratified, with cold, heavily sea ice-loaded surface waters and strong influx of warm waters in the subsurface. High surface water productivity suggests that the polar front was close to our location.
- A short-lived peak in terrestrially-derived elements suggesting transport of sediments from land via meltwater or icebergs may be linked to the so-called 8.2 ka BP event.
- The interval from 8.2 to 6.2 ka BP was characterised by the warmest bottom-water conditions of the Holocene on the NE Greenland shelf, with low surface water productivity and strong AW influence (RAC) in the weakened EGC.
- After the HTM the water column started the resemble that of the period prior to 8.2 ka BP. The EGC became stronger, with sea-ice loaded surface waters and relatively warm Atlantic-sourced subsurface waters. The subsurface inflow of warm AW from the RAC decreased, but remained persistent.
- After 4.2 ka BP increased PW at the surface of the EGC and reduction of the RAC at subsurface levels led to freshening and reduced stratification of the water column and (near) perennial sea-ice cover.
- The period from ca. 3.2 until 0.3 ka BP is characterised by cold and unstable conditions, with minimum surface water productivity, and possible sea-ice cover at our location. During this period, the EGC was likely strengthened, with a thick layer of cold and fresh PW on the surface and strong recirculated AAW inflow from the Arctic at subsurface levels.
- The proportion of PW and AW in the EGC shows a strong covariance with the northward heat transport to the northern North Atlantic. Thus, the cooling trend that characterizes the Holocene after the HTM led to strengthened EGC and increased PW transport, probably due to transition to a negative NAO phase. This stronger and fresher EGC in the late-Holocene is likely to have impacted the Subpolar Gyre circulation and helped to strengthen the AMOC

Appendices

Table A1: Foraminiferal taxa identified in this study (core depth 345-0 cm), with their original reference. Benthic calcareous, agglutinated and planktic species are separate and listed alphabetically.

Benthic agglutinated

https://doi.org/10.5194/cp-2021-59
Preprint. Discussion started: 2 June 2021


Climate of the Past Discussions

Adercotryma glomerata (Brady, 1878)
Ammodiscus sp.
Ammoglobogerina globigeriniformis (Parker and Jones, 1865)
Cibrostomoides kosterensis (Höglund, 1947)
Deuterammina grahami (Brönnimann and Whittaker, 1988)
Deuterammina montagui (Brönnimann and Whittaker, 1988)
Hormosinella sp.
Portatrochammina bipolaris (Brönnimann and Whittaker, 1980)
Recurvoides turbinatus (Brady, 1881)
Reophax fusiformis (Williamson, 1858)
Reophax guttifer/rostrata (Brady, 1881)/(Höglund, 1947)
Reophax sp.
Reophax subfusiformis (Earland, 1933)
Rhabdammina sp.
Saccammina difflugiformis (Brady, 1879)
Saccammina sphaerica (Brady, 1871)
Saccorhiza ramosa (Brady, 1879)
Spiroplectammina biformis (Parker and Jones, 1865)
Textularia cf. *earlandi* (Parker, 1952)
Textularia torquata (Parker, 1952)
Texularia kattagatensis (Höglund, 1948)

Benthic calcareous
Islandiella helanae (Feyling-Hanssen and Buzas, 1976)
Ammonia sp.
Astrononion gallowayi (Loeblich and Tappan, 1953)
Bolivina aff. albatrossi (Cushman, 1922)
Buccella frigida (Cushman, 1922)
Buliminella elegantissima (d´Orbigny, 1839)
Cassidulina neoteretis (Seidenkrantz, 1995)
Cassidulina reniforme (Nørvang, 1945)
Ceratobulimina arctica (Green, 1959)
Cibicides lobatulus (Walker and Jacob, 1798)
Dentalina pauperata (d´Orbigny, 1846)
Elphidium albiumbilicatum (Weiss, 1964)
Elphidium clavatum (Cushman, 1930)
Elphidium frigidum (Cushman, 1933)
Elphidium hallandense (Brotzen, 1943)
Eoponidella pulchella (Parker, 1952)
Epistominella arctica (Green, 1959)
Epistominella vitrea (Parker, 1953)
Fisurina sp.
Florius sp.
Glabratella arctica (Scott and Vilks, 1991)
Globulina oculus (Jennings, Seidenkrantz and Knudsen, 2020)
Guttulina glacialis (Cushman and Ozawa, 1930)
Haynesina nivea (Lafrenz, 1963)
Islandiella norcrossi (Cushman, 1933)

https://doi.org/10.5194/cp-2021-59
Preprint. Discussion started: 2 June 2021


Climate of the Past Discussions

Lagena sp./*Procerolagena*
Melonis barleeanum (Williamson, 1858)
Miliolinella subrotunda (Montague, 1803)
Nonionella iridea (Heron-Allen and Earland, 1932)
Nonionella labradorica (Dawson, 1860)
Polymorphina sp.
Pullenia bulloides (d´Orbigny, 1846)
Pyrgo williamsoni (Silvestri, 1923)
Quinqueloculina seminulum (Linnaeus, 1758)
Quniqueloculina stalkeri (Loeblich and Tappan, 1953)
Robertina arctica (d´Orbigny, 1846)
Sagrina sp.
Stainforthia concava (Höglund, 1947)
Stainforthia feylingi (Knudsen and Seidenkrantz, 1994)
Stainforthia fusiformis (Williamson, 1858)
Stetsonia horvathi (Green, 1959)
Trifarina fluens (Todd in Cushman and McCulloch, 1948)
Triloculina tricarinata (d´Orbigny, 1846)
Triloculina trihedra (Loebich and Tappan, 1953)

Planktic
Neogloboquadrina incompta (Cifelli, 1961)
Neogloboquadrina pachyderma (Ehrenberg, 1861)
Turborotalita quinqueloba (Natland, 1938)

555 **Table A2: List of benthic foraminiferal key species used for paleoenvironmental reconstruction.**

Species	Environmental preferences	References
Calcareous		
Cassidulina neoteretis	warm, saline Atlantic Water	Mackensen and Hald, 1988; Seidenkrantz, 1995; Rytter et al., 2002; Jennings et al., 2004; Jennigns et al., 2011, Perner et al., 2015; Cage et al., 2021
Pullenia bulloides	warm, saline Atlantic Water	Rytter et al., 2002; Jennings et al., 2011
Islandiella norcrossi	chilled Atlantic Water	Slubowska-Woldengen et al., 2007; Perner et al., 2011; Perner et al., 2015
Melonis barleeanum	productivity, cool Atlantic Water	Perner et al., 2015
Stetsonia horvathi	cold, Arctic deep water	Green, 1960; Lagoe, 1979; Wollenburg and Mackensen, 1988; Jennings et al., 2020
Epistominella arctica	cold, Arctic deep water, productivity	Green, 1960; Lagoe, 1979; Wollenburg and Mackensen, 1988; Jennings et al., 2020
Stainforthia feylingi	tolerates unstable conditions and low bottom-water oxygen, high productivity, often in sea-ice edge regions	Knudsen and Seidenkrantz, 1994

https://doi.org/10.5194/cp-2021-59
Preprint. Discussion started: 2 June 2021

Agglutinated		
Adercotryma glomerata	Atlantic sourced waters	Hald and Korsun, 1997, Lloyd 2006; Perner et al., 2012; Wangner et al., 2018
Textularia earlandi	cold, low-salinity Arctic waters	Jennings and Helgadottir, 1994; Korsun and Hald, 2000; Wangner et al., 2018
Textularia torquata	cold, low-salinity Arctic waters	Perner et al., 2012; Perner et al., 2015; Wangner et al., 2018
Spiroplectammina biformis	cold, low-salinity Arctic waters	Jennings and Helgadottir, 1994; Korsun and Hald, 2000; Perner et al., 2012; Wangner et al., 2018
Saccammina difflugiformis	Polar Waters on the EG shelf	Jennings and Helgadottir, 1994

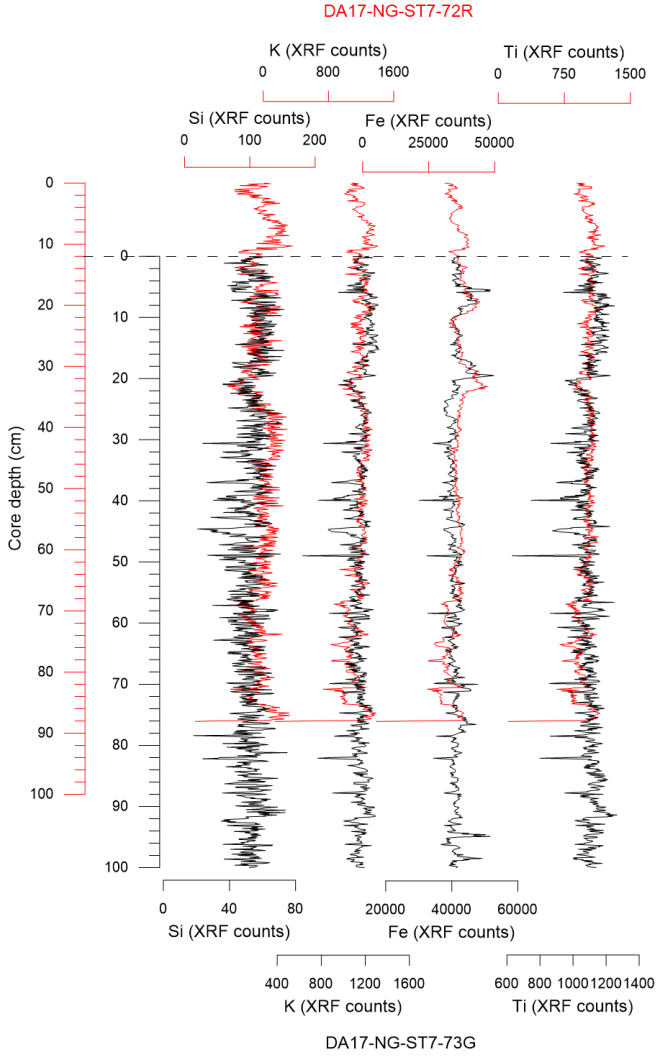

Figure A1: Comparison of XRF data from gravity core DA17-NG-ST7-73G (black) and Rumohr core DA17-NG-ST7-72R (red).

https://doi.org/10.5194/cp-2021-59
Preprint. Discussion started: 2 June 2021

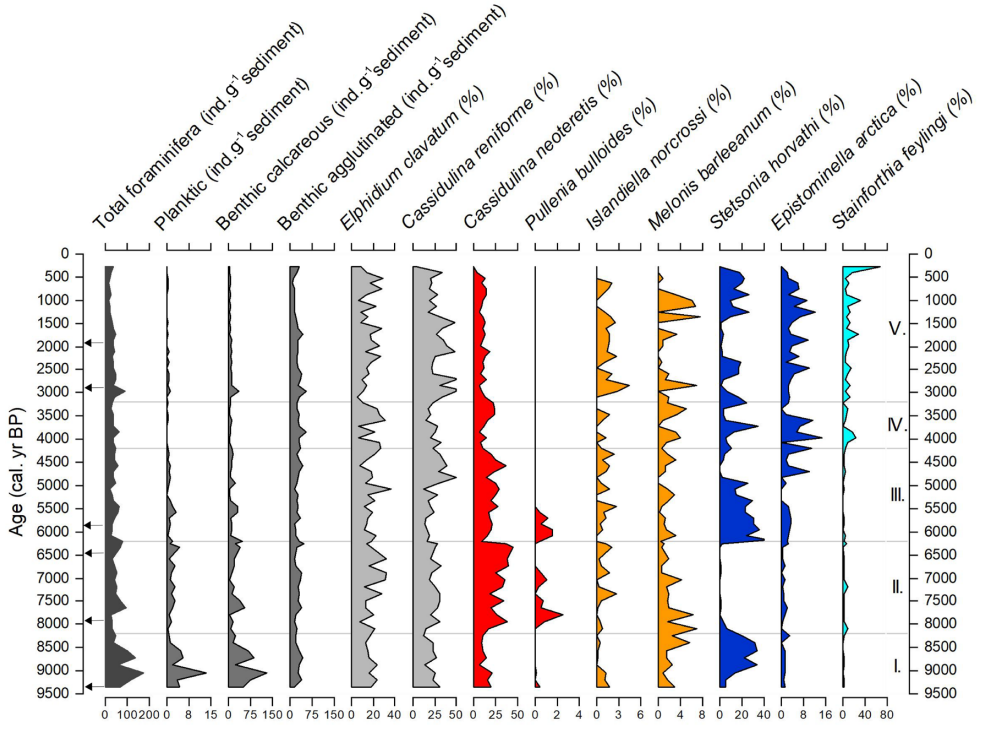

560

Figure A2: Foraminferal concentrations and relative abundances of nine selected benthic calcareous species (expressed as a percentage of total benthic calcareous foraminiferal content) versus calibrated age along sediment core DA17-NG-ST7-73G. The depicted species were chosen in order to show changes in the environment. Red colour represents species that indicate warm Atlantic Water inflow; orange represents species that indicate in the Arctic recirculated, chilled Atlantic Water influence; dark blue represents Artic Water 565 **species; light blue represents a species that indicates sea ice. Ecozones (I.-V.) are shown on the right side of the figure. Black arrows next to the left y-axis mark radiocarbon dates. Note that the x-axes have different scaling.**

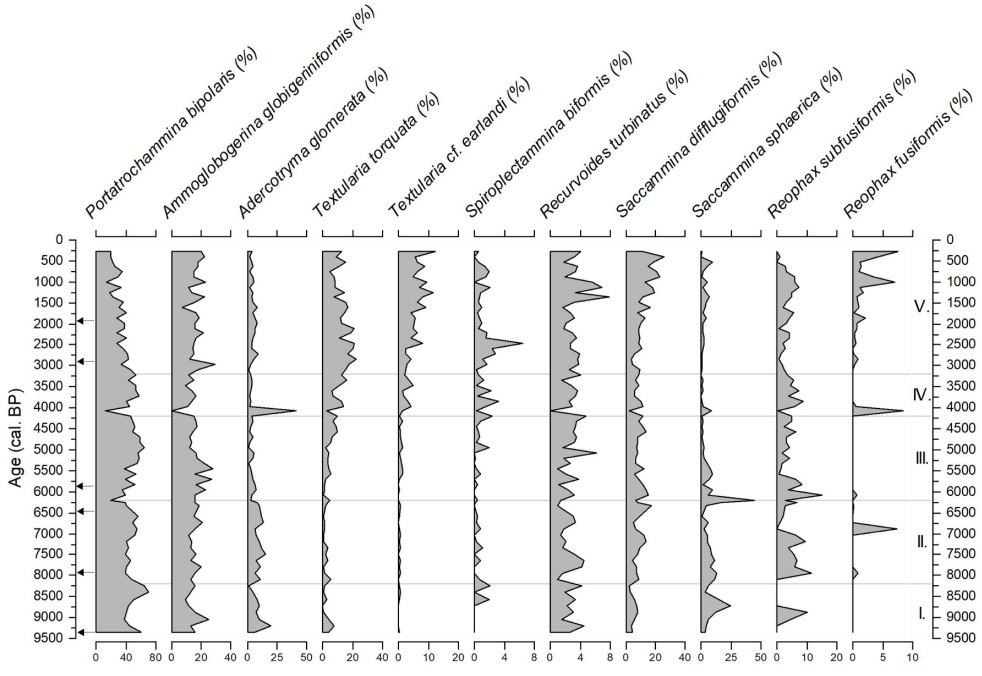

https://doi.org/10.5194/cp-2021-59
Preprint. Discussion started: 2 June 2021

Figure A3: Relative abundances of the most abundant (>5% in at least one sample) benthic agglutinated foraminifera species (expressed as a percentage of total benthic agglutinated foraminiferal content) versus calibrated age along sediment core DA17-NG-ST7-73G. Ecozones (I.-V.) are shown on the right side of the figure. Black arrows next to the left y-axis mark radiocarbon dates. Note that the x-axes have different scaling.

Data availability

Data presented in this manuscript have been uploaded to PANGEA (under review).

Author contribution

Teodora Pados-Dibattista and Marit-Solveig Seidenkrantz developed the research idea. Teodora Pados-Dibattista carried out the sampling, data collection and the data analysis, with the help of Christof Pearce, Henrieka Detlef, Jørgen Brendtsen and Marit-Solvieg Seidenkrantz. Christof Pearce performed the age modelling of the core. Teodora Pados-Dibattista prepared the manuscript with contributions from all co-authors.

Competing interests

Author Marit-Solveig Seidenkrantz is co-editor-in-chief of the journal.

Acknowledgements

We would like to thank the captain and crew as well as the shipboard scientific party onboard RV *Dana*. We also wish to thank Marianne Lyngholm Nielsen for carrying out the X-Ray Fluorescence core scanning and the magnetic susceptibility measurements and Nils Andersen, Leibniz Laboratory for Radiometric Dating and Stable Isotope Research at the Christian-Albrechts-University of Kiel, for the stable isotope measurements.

Financial support

The NorthGreen17 expedition was funded by the Danish Centre for Marine Research and the Natural Science and Engineering Research Council of Canada. The research was funded by the European Union´s Horizon 2020 research and innovation programme under grant agreement No. 792639, with further support from the Danish Council for Independent Research (grants no. 7014- 00113B (G-Ice) and 0135-00165B (GreenShelf) to MSS)) and the European Union's Horizon 2020 research and innovation program under grant agreement No. 869383 (ECOTIP).

References

Alley, R. B., Mayewski, P. A., Sowers, T., Stuiver, M., Taylor, K. C., and Clark, P. U.: Holocene climatic instability: A prominent, widespread event 8200 yr ago, Geology, 25(6), 483-486, 1997.

Andersen, C., Koç, N., Jennings, A. E., and Andrews, J. T.: Nonuniform response of the major surface currents in the Nordic Seas to insolation forcing: Implications for the Holocene climate variability, Paleoceanography, 19, PA2003, https://doi:10.1029/2002PA000873, 2004.

https://doi.org/10.5194/cp-2021-59
Preprint. Discussion started: 2 June 2021

Andrews, J. T., Smith, L. M., Preston, R., Cooper, T., and Jennings, A. E.: Spatial and temporal patterns of iceberg rafting (IRD) along the East Greenland margin, ca. 68 N, over the last 14 cal. Ka, J. Quaternary Sci.: Published for the Quaternary Research Association, 12(1), 1-13, 1997.

Arndt, J. E., Jokat, W., Dorschel, B., Myklebust, R., Dowdeswell, J. A., and Evans, J.: A new bathymetry of the Northeast Greenland continental shelf: Constraints on glacial and other processes, Geochem. Geophy. Geosy., 16(10), 3733-3753, 2015.

Arndt, J. E., Jokat, W., and Dorschel, B.: The last glaciation and deglaciation of the Northeast Greenland continental shelf revealed by hydro-acoustic data, Quaternary Sci. Rev., 160, 45–56, 2017.

Barber, D. C., Dyke, A., Hillaire-Marcel, C., Jennings, A. E., Andrews, J. T., Kerwin, M. W., Bilodeau, G., McNeely, R., Southon, J., Morehead, M. D., and Gagnon, J.-M.: Forcing of the cold event of 8,200 years ago by catastrophic drainage of Laurentide lakes, Nature, 400(6742), 344-348, 1999.

Bauch, H. A., Erlenkeuser, H., Spielhagen, R. F., Struck, U., Matthiessen, J., Thiede, J., and Heinemeier, J.: A multiproxy reconstruction of the evolution of deep and surface waters in the subarctic Nordic seas over the last 30,000 yr., Quaternary Sci. Rev., 20(4), 659-678, 2001.

Bennike, O. L. E. and Weidick, A.: Late Quaternary history around Nioghalvfjerdsfjorden and Jøkelbugten, North-East Greenland, Boreas, 30(3), 205-227, 2001.

Berger, A.: Long-term variations of caloric insolation resulting from the Earth's orbital elements, Quaternary Res., 9(2), 139-167, 1978.

Blaschek, M. and Renssen, H.: The Holocene thermal maximum in the Nordic Seas: the impact of Greenland Ice Sheet melt and other forcings in a coupled atmosphere–sea-ice–ocean model, Clim. Past, 9(4), 1629-1643, 2013.

Bourke, R. H., Newton, J. L., Paquette, R. G., and Tunnicliffe, M. D.: Circulation and water masses of the East Greenland shelf, J. Geophys. Res., 92(C7), 6729–6740, https://doi:10.1029/JC092iC07p06729, 1987.

Boyer, T. P., Garcia, H., E, Locarnini, R. A., Ricardo, A., Zweng, M. M., Mishonov, A. V., Reagan, J., R., Weathers, K., A., Baranova, O. K., Seidov, D., and Smolyar, I. V.: World Ocean Atlas 2018, NOAA National Centers for Environmental Information, dataset, https://accession.nodc.noaa.gov/NCEI-WOA18, 2018.

Cabedo-Sanz, P., Belt, S. T., Jennings, A. E., Andrews, J. T., and Geirsdóttir, Á.: Variability in drift ice export from the Arctic Ocean to the North Icelandic Shelf over the last 8000 years: a multi-proxy evaluation, Quaternary Sci. Rev., 146, 99-115, 2016.

Caesar, L., McCarthy, G. D., Thornalley, D. J. R., Cahill, N., and Rahmstorf, S.: Current Atlantic Meridional Overturning Circulation weakest in last millennium, Nat. Geosci., 1-3, https://doi: 10.1038/s41561-021-00699-z, 2021.

Cage, A.G., Pieńkowski, A.J., Jennings, A., Knudsen, K.L., and Seidenkrantz, M.-S.: Comparative analysis of six common foraminiferal species of the genera *Cassidulina*, *Paracassidulina* and *Islandiella* from the Arctic-North Atlantic domain, J. Micropalaeontol., in press, 2021.

Clark, P. U., Marshall, S. J., Clarke, G. K., Hostetler, S. W., Licciardi, J. M., and Teller, J. T.: Freshwater forcing of abrupt climate change during the last glaciation, Science, 293(5528), 283-287, 2001.

Clark, P. U., Pisias, N. G., Stocker, T. F., and Weaver, A. J.: The role of the thermohaline circulation in abrupt climate change, Nature, 415(6874), 863-869, 2002.

Consolaro, C., Rasmussen, T. L., and Panieri, G.: Palaeoceanographic and environmental changes in the eastern Fram Strait during the last 14,000 years based on benthic and planktonic foraminifera, Mar. Micropaleontol., 139, 84-101, 2018.

Cronin, T. M., Dwyer, G. S., Kamiya, T., Schwede, S., and Willard, D. A.: Medieval warm period, little ice age and 20th century temperature variability from Chesapeake Bay, Global Planet. Change, 36(1-2), 17-29, 2003.

https://doi.org/10.5194/cp-2021-59
Preprint. Discussion started: 2 June 2021

Danish Meteorological Institute (DMI) and NSIDC: Arctic Sea Ice Charts from the Danish Meteorological Institute, 1893-1995, edited by: Underhill, V., Fetterer, F., National Snow and Ice Data Center, Boulder, Colorado USA, 2012.

Ellison, C. R. W., Chapman, M. R., and Hall, I. R.: Surface and deep ocean interactions during the cold climate event 8200 years ago, Science, 312(5782), 1929–1932, https://doi.org/10.1126/science.1127213, 2006.

Estrade, P., Marchesiello, P., Colin De Verdiere, A., and Roy, C.: Cross-shelf structure of coastal upwelling: A two-dimensional extension of Ekman's theory and a mechanism for inner shelf upwelling shut down, J. Mar. Res., 66, 589–616, https://doi:10.1357/002224008787536790, 2008.

Feyling-Hanssen, R. W.: The stratigraphy of the Quaternary Clyde Foreland Formation, Baffin Island, illustrated by the distribution of benthic foraminifera, Boreas, 5, 77–94, 1976.

Feyling-Hanssen, R. W.: Microbiostratigraphy of young Cenozoic marine deposits of Qivituq Peninsula, Baffin Island, Mar. Micropaleontol., 5, 153–184, 1980.

Feyling-Hanssen, R., Funder, S., and Petersen, K.S.: The Lodin Elv Formation; a Plio-Pleistocene occurrence in Greenland, B. Geol. Soc. Den., 31, 81–106, 1983.

Funder, S., Bennike, O., Böcher, J., Israelson, C., Strand Petersen, K., and Símonarson, L. A.: Late Pliocene Greenland–The Kap København Formation in North Greenland, B. Geol. Soc. Den., 48, 117-134, 2001.

Giraudeau, J., Jennings, A. E., and Andrews, J. T.: Timing and mechanisms of surface and intermediate water circulation changes in the Nordic Seas over the last 10,000 cal years: a view from the North Iceland shelf, Quaternary Sci. Rev., 23(20-22), 2127-2139, 2004.

Giraudeau, J., Grelaud, M., Solignac, S., Andrews, J. T., Moros, M., and Jansen, E.: Millennial-scale variability in Atlantic water advection to the Nordic Seas derived from Holocene coccolith concentration records, Quaternary Sci. Rev., 29(9-10), 1276-1287, 2010.

Green, K. E.: Ecology of some Arctic foraminifera, Micropaleontol., 6, 57–78, 1960.

Hald, M. and Korsun, S.: Distribution of modern benthic foraminifera from fjords of Svalbard, European Arctic, J. Foramin. Res., 27(2), 101-122, 1997.

Hald, M., Andersson, C., Ebbesen, H., Jansen, E., Klitgaard-Kristensen, D., Risebrobakken, B., Salomonsen, G. R., Sarnthein, M., Sejrup, H. P., and Telford, R. J.: Variations in temperature and extent of Atlantic Water in the northern North Atlantic during the Holocene, Quaternary Sci. Rev., 26(25-28), 3423-3440, 2007.

Hall, I. R., Bianchi, G. G., and Evans, J. R.: Centennial to millennial scale Holocene climate-deep water linkage in the North Atlantic. Quaternary Sci. Rev., 23(14-15), 1529-1536, 2004.

Heaton, T. J., Köhler, P., Butzin, M., Bard, E., Reimer, R. W., Austin, W. E. N., Bronk Ramsey, C., Grootes, P. M., Hughen, K. A., Kromer, B., Reimer, P. J., Adkins, J., Burke, A., Cook, M. S., Olsen, J., and Skinner, L. C.: Marine20—The Marine Radiocarbon Age Calibration Curve (0–55,000 Cal BP), Radiocarbon, 62(4), 779–820, https://doi.org/10.1017/RDC.2020.68, 2020.

Hillaire-Marcel, C., De Vernal, A., Bilodeau, G., and Weaver, A. J.: Absence of deep-water formation in the Labrador Sea during the last interglacial period, Nature, 410(6832), 1073-1077, 2001.

Hillaire-Marcel, C., De Vernal, A., and Piper, D. J.: Lake Agassiz final drainage event in the northwest North Atlantic, Geophys. Res. Lett., 34(15), 2007.

Hoffman, J. S., Carlson, A. E., Winsor, K., Klinkhammer, G. P., LeGrande, A. N., Andrews, J. T., and Strasser, J. C.: Linking the 8.2 ka event and its freshwater forcing in the Labrador Sea, Geophys. Res. Lett., 39(18), 2012.

https://doi.org/10.5194/cp-2021-59
Preprint. Discussion started: 2 June 2021

Hurrell, J. W. and Deser, C.: North Atlantic climate variability: the role of the North Atlantic Oscillation, J. Marine Syst., 79(3-4), 231-244, 2010.

Hurrell, J. W., Kushnir, Y., Ottersen, G., and Visbeck, M.: An overview of the North Atlantic oscillation. Geophysical Monograph-American Geophysical Union, 134, 1-36, 2003.

Ionita, M., Scholz, P., Lohmann, G., Dima, M., and Prange, M.: Linkages between atmospheric blocking, sea ice export through Fram Strait and the Atlantic meridional overturning circulation, Sci. Rep.-UK, 6, 32881, https://doi.org/10.1038/srep32881, 2016.

Jansen, E., Andersson, C., Moros, M., Nisancioglu, K. H., Nyland, B. F., and Telford, R. J.: The Early to Mid-Holocene Thermal Optimum in the North Atlantic, in: Natural Climate Variability and Global Warming, edited by: Battarbee, R. W., Binney, H. A., Wiley Blackwell, 123–137, https://doi:10.1002/9781444300932.ch5, 2008.

Jennings, A. E. and Helgadottir, G.: Foraminiferal assemblages from the fjords and shelf of eastern Greenland. J. Foramin. Res., 24(2), 123-144, 1994.

Jennings, A. E., Knudsen, K. L., Hald, M., Hansen, C. V., and Andrews, J. T.: A mid-Holocene shift in Arctic sea-ice variability on the East Greenland Shelf, The Holocene, 12(1), 49-58, 2002.

Jennings, A. E., Weiner, N. J., Helgadottir, G., and Andrews, J. T.: Modern foraminiferal faunas of the southwestern to northern Iceland shelf: oceanographic and environmental controls, J. Foramin. Res., 34(3), 180-207, 2004.

Jennings, A., Andrews, J., and Wilson, L.: Holocene environmental evolution of the SE Greenland Shelf North and South of the Denmark Strait: Irminger and East Greenland current interactions, Quaternary Sci. Rev., 30(7-8), 980-998, 2011.

Jennings, A., Andrews, J., Reilly, B., Walczak, M., Jakobsson, M., Mix, A., Stoner, J., Nicholls, K. W., and Cheseby, M.: Modern foraminiferal assemblages in northern Nares Strait, Petermann Fjord, and beneath Petermann ice tongue, NW Greenland, Arct. Antarct. Alp. Res., 52(1), 491-511, 2020.

Johanessen, O. M.: Brief overview of the physical oceanography, in: The Nordic Seas, edited by: Hurdle, B.G., Springer-Verlag, New York, https://doi.org/10.1007/978-1-4615-8035-5_4, 1986.

Kaufmann, D. S., Ager, T. A., Anderson, N. J., Anderson, P. M., Andrews, J. T., Bartlein, P. J., Brubaker, L. B., Coats, L. L., Cwynar, L. C., Duvall, M. L., Dyke, A. S., Edwards, M. E., Eisner, W. R., Gajewski, K., Geirsdóttir, A., Hu, F. S., Jennings, A. E., Kaplan, M. R., Kerwin, M. W., Lozhkin, A. V., MacDonald, G. M., Miller, G. H., Mock, C. J., Oswald, W. W., Otto-Bliesner, B. L., Porinchu, D. F., Rühland, K., Smol, J. P., Steig, E. J., and Wolfe, B. B.: Holocene thermal maximum in the western Arctic (0-180°W), Quaternary Sci. Rev., 23, 529–560, 2004.

Keigwin, L. D., Sachs, J. P., Rosenthal, Y., and Boyle, E. A.: The 8200 year B.P. event in the slope water system, western subpolar North Atlantic, Paleoceanography, 20, https://dx.doi.org/10.1029/2004PA001074, 2005.

Kirillov, S., Dmitrenko, I., Tremblay, B., Gratton, Y., Barber, D., and Rysgaard, S.: Upwelling of Atlantic Water along the Canadian Beaufort Sea continental slope: Favorable atmospheric conditions and seasonal and interannual variations, J. Clim., 29(12), 4509-4523, https://doi.org/10.1175/JCLI-D-15-0804.1, 2016.

Knudsen, K. L. and Seidenkrantz, M. S.: *Stainforthia feylingi* new species from arctic to subarctic environments, previously recorded as *Stainforthia schreibersiana* (Czjzek). Cushman Foundation for Foraminiferal Research Special Publication, 32, 5-13, 1994.

Knudsen, M. F., Seidenkrantz, M. S., Jacobsen, B. H., and Kuijpers, A.: Tracking the Atlantic Multidecadal Oscillation through the last 8,000 years, Nat. Commun., 2(1), 1-8, 2011.

Koç, N., Jansen, E., and Haflidason, H.: Paleoceanographic reconstructions of surface ocean conditions in the Greenland, Iceland and Norwegian seas through the last 14 ka based on diatoms, Quaternary Sci. Rev., 12, 115–40, 1993.

https://doi.org/10.5194/cp-2021-59
Preprint. Discussion started: 2 June 2021

715 Kolling, H. M., Stein, R., Fahl, K., Perner, K., and Moros, M.; Short-term variability in late Holocene sea ice cover on the East Greenland Shelf and its driving mechanisms, Palaeogeogr. Palaeocl., 485, 336-350, 2017.

Korsun, S. and Hald, M.: Seasonal dynamics of benthic foraminifera in a glacially fed fjord of Svalbard, European Arctic, J. Foramin. Res., 30(4), 251-271, 2000.

Kwok, R.: Recent changes in Arctic Ocean sea ice motion associated with the North Atlantic Oscillation, Geophys. Res. Lett., 720 27(6), 775-778, 2000.

Lagoe, M. B.: Recent Benthic foraminifera from the Central Arctic Ocean, J. Foramin. Res., 7, 106–129, 1979.

Larsen, N. K., Levy, L. B., Carlson, A. E., Buizert, C., Olsen, J., Strunk, A., Bjørk, A. A., and Skov, D. S.: Instability of the Northeast Greenland Ice Stream over the last 45,000 years, Nat. Commun., 9(1), 1-8, 2018.

Lloyd, J. M.: Modern distribution of benthic foraminifera from Disko Bugt, West Greenland, J. Foramin. Res., 36(4), 315-331, 725 2006.

Mackensen, A. and Hald, M.: *Cassidulina teretis* Tappan and *C. laevigata* D'Orbigny: their modern and Late Quaternary distribution in Northern seas, J. Foramin. Res., 18(1), 16–24, 1988.

Mayer, C., Reeh, N., Jung-Rothenhäusler, F., Huybrechts, P., and Oerter, H.: The subglacial cavity and implied dynamics under Nioghalvfjerdsfjorden Glacier, NE-Greenland, Geophys. Res. Lett., 27(15), 2289-2292, 2000.

730 Moossen, H., Bendle, J., Seki, O., Quillmann, U., and Kawamura, K.: North Atlantic Holocene climate evolution recorded by high-resolution terrestrial and marine biomarker records, Quaternary Sci. Rev., 129, 111e127, 2015.

Moros, M., Jansen, E., Oppo, D. W., Giraudeau, J., and Kuijpers, A.: Reconstruction of the late-Holocene changes in the Sub-Arctic Front position at the Reykjanes Ridge, north Atlantic, The Holocene, 22(8), 877-886, 2012.

Müller, J., Werner, K., Stein, R., Fahl, K., Moros, M., and Jansen, E.: Holocene cooling culminates in sea ice oscillations in Fram 735 Strait, Quaternary Sci. Rev., 47, 1-14, 2012.

Oppo, D. W., McManus, J. F., and Cullen, J. L.: Deepwater variability in the Holocene epoch, Nature, 422(6929), 277-277, 2003.

Orme, L. C., Miettinen, A., Divine, D., Husum, K., Pearce, C., Van Nieuwenhove, N., Born, A., Mohan, R., and Seidenkrantz, M. S.: Subpolar North Atlantic sea surface temperature since 6 ka BP: Indications of anomalous ocean-atmosphere interactions at 4-2 ka BP, Quaternary Sci. Rev., 194, 128-142, 2018.

740 Pedersen, L.T., Gudmandsen, P., and Skriver, H.: North-East Water - A remote sensing study, Report 545, Electromagnetic Institute, Technical University of Denmark, 1993.

Perner, K., Moros, M., Lloyd, J. M., Kuijpers, A., Telford, R. J., and Harff, J.: Centennial scale benthic foraminiferal record of late Holocene oceanographic variability in Disko Bugt, West Greenland, Quaternary Sci. Rev., 30(19-20), 2815-2826, 2011.

Perner, K., Moros, M., Jennings, A., Lloyd, J. M., and Knudsen, K. L.: Holocene palaeoceanographic evolution off West 745 Greenland, The Holocene, 23(3), 374-387, 2012.

Perner, K., Moros, M., Lloyd, J. M., Jansen, E., and Stein, R.: Mid to late Holocene strengthening of the East Greenland Current linked to warm subsurface Atlantic water, Quaternary Sci. Rev., 129, 296-307, 2015.

Perner, K., Jennings, A. E., Moros, M., Andrews, J. T., and Wacker, L.: Interaction between warm Atlantic-sourced waters and the East Greenland Current in northern Denmark Strait (68 N) during the last 10 600 cal a BP, J. Quaternary Sci., 31(5), 472-483, 750 2016.

Quadfasel, D., Gascard, J. C., and Koltermann, K. P.: Large-scale oceanography in Fram Strait during the 1984 marginal ice zone experiment, J. Geophys. Res.-Oceans, 92, 6719-6728, 1987.

Rahmstorf, S.: Bifurcations of the Atlantic thermohaline circulation in response to changes in the hydrological cycle, Nature, 378(6553), 145-149, 1995.

https://doi.org/10.5194/cp-2021-59
Preprint. Discussion started: 2 June 2021

Ramsey, C. B.: Deposition models for chronological records. Quaternary Sc. Rev., 27(1-2), 42-60, 2008.

Ran, L., Jiang, H., Knudsen, K. L., Eiríksson, J., and Gu, Z.: Diatom response to the Holocene climatic optimum on the North Icelandic shelf, Mar. Micropaleontol., 60(3), 226-241, 2006.

Rasmussen, S. O., Vinther, B. M., Clausen, H. B., and Andersen, K. K.: Early Holocene climate oscillations recorded in three Greenland ice cores, Quaternary Sci. Rev., 26, 1907–1914, https://doi.org/10.1016/j.quascirev.2007.06.015, 2007.

Reimer, P. J. and Reimer, R. W.: A marine reservoir correction database and on-line interface, Radiocarbon, 43(2A), 461-463, 2001.

Renssen, H., Goosse, H., and Muscheler, R.: Coupled climate model simulation of Holocene cooling events: oceanic feedback amplifies solar forcing, Clim. Past, 2(2), 79-90, 2006.

Risebrobakken, B., Jansen, E., Andersson, C., Mjelde, E., and Hevrøy, K.: A high-resolution study of Holocene paleoclimatic and paleoceanographic changes in the Nordic Seas, Paleoceanography, 18(1), 2003.

Risebrobakken, B., Dokken, T., Smedsrud, L. H., Andersson, C., Jansen, E., Moros, M., and Ivanova, E. V.: Early Holocene temperature variability in the Nordic Seas: The role of oceanic heat advection versus changes in orbital forcing, Paleoceanography, 26(4), PA4206, https://doi:10.1029/2011PA002117, 2011.

Rudels, B.: Arctic Ocean circulation and variability–advection and external forcing encounter constraints and local processes, Ocean Sci., 8(2), 261-286, 2012.

Rudels, B. and Quadfasel, D.: Convection and deep water formation in the Arctic Ocean-Greenland Sea system, J. Marine Syst., 2(3-4), 435-450, 1991.

Rudels, B., Björk, G., Nilsson, J., Winsor, P., Lake, I., and Nohr, C.: The interaction between waters from the Arctic Ocean and the Nordic Seas north of Fram Strait and along the East Greenland Current: results from the Arctic Ocean-02 Oden expedition, J. Marine Syst., 55(1-2), 1-30, 2005.

Rytter, F., Knudsen, K. L., Seidenkrantz, M. S., and Eiríksson, J.: Modern distribution of benthic foraminifera on the North Icelandic shelf and slope, J. Foramin. Res., 32(3), 217-244, 2002.

Sachs, J.P.: Cooling of Northwest Atlantic slope waters during the Holocene, Geophys. Res. Lett., 34, L03609, http://dx.doi.org/10.1029/2006GL028495, 2007.

Sarthein, M., Van Kreveld, S., Erlenkeuser, H., Grootes, P. M., Kucera, M., Pflaumann, U., and Schulz, M.: Centinnal-to-millenial-scale periodicities of Holocene climate and sediment injections off the western Barents shelf, 75 N, Boreas, 32(3), 447-461, 2003.

Schaffer, J., von Appen, W. J., Dodd, P. A., Hofstede, C., Mayer, C., de Steur, L., and Kanzow, T.: Warm water pathways toward Nioghalvfjerdsfjorden Glacier, Northeast Greenland. J. Geophys. Res.-Oceans, 122(5), 4004-4020, 2017.

Schneider, W. and Budéus, G.: The northeast water polynya (Greenland Sea), Polar Biol., 14(1), 1-9, 1994.

Schneider, W. and Budéus, G.: Summary of the Northeast Water polynya formation and development (Greenland Sea), J. Marine Syst., 10(1-4), 107-122, 1997.

Seidenkrantz, M. S.: *Cassidulina teretis* Tappan and *Cassidulina neoteretis* new species (Foraminifera): stratigraphic markers for deep sea and outer shelf areas, J. Micropalaeontol., 14(2), 145-157, 1995.

Seidenkrantz, M. S.: Benthic foraminifera as palaeo sea-ice indicators in the subarctic realm – examples from the Labrador Sea – Baffin Bay region, Quaternary Sci. Rev., 79, 135–144; https://doi: 10.1016/j.quascirev.2013.03.014, 2013.

Seidenkrantz, M. S., Aagaard-Sørensen, S., Sulsbrück, H., Kuijpers, A., Jensen, K. G., and Kunzendorf, H.: Hydrography and climate of the last 4400 years in a SW Greenland fjord: implications for Labrador Sea palaeoceanography, The Holocene, 17(3), 387-401, 2007.

https://doi.org/10.5194/cp-2021-59
Preprint. Discussion started: 2 June 2021

Seidenkrantz, M. S., Roncaglia, L., Fischel, A., Heilmann-Clausen, C., Kuijpers, A., and Moros, M.: Variable North Atlantic climate seesaw patterns documented by a late Holocene marine record from Disko Bugt, West Greenland, Mar. Micropaleontol., 68(1-2), 66-83, 2008.

Seidenkrantz, M. S., Ebbesen, H., Aagaard-Sørensen, S., Moros, M., Lloyd, J. M., Olsen, J., Knudsen, M. F. and Kuijpers, A.: Early Holocene large-scale meltwater discharge from Greenland documented by foraminifera and sediment parameters, Palaeogeogr. Palaeocl., 391, 71-81, 2013.

Seidenkrantz, M.-S., Kuijpers, A., Olsen, J., Pearce, C., Lindblom, S., Ploug, J., Przybyło, P., and Snowball, I.: Southwest Greenland shelf glaciation during MIS 4 more extensive than during the Last Glacial Maximum, Sci. Rep.-UK, 9, 15617; https://doi: 10.1038/s41598-019-51983-3, 2019.

Ślubowska-Woldengen, M., Rasmussen, T. L., Koc, N., Klitgaard-Kristensen, D., Nilsen, F., and Solheim, A.: Advection of Atlantic Water to the western and northern Svalbard shelf since 17,500 cal yr BP. Quaternary Sci. Rev., 26(3-4), 463-478, 2007.

Stroeve, J. C., Serreze, M. C., Holland, M. M., Kay, J. E., Malanik, J., and Barrett, A. P.: The Arctic's rapidly shrinking sea ice cover: a research synthesis, Climatic Change, 110(3), 1005-1027, 2012.

Syring, N., Stein, R., Fahl, K., Vahlenkamp, M., Zehnich, M., Spielhagen, R. F., and Niessen, F.: Holocene changes in sea-ice cover and polynya formation along the eastern North Greenland shelf: New insights from biomarker records, Quaternary Sci. Rev., 231, 106173, 2020a.

Syring, N., Lloyd, J. M., Stein, R., Fahl, K., Roberts, D. H., Callard, L., and O'Cofaigh, C.: Holocene Interactions Between Glacier Retreat, Sea Ice Formation, and Atlantic Water Advection at the Inner Northeast Greenland Continental Shelf, Paleoceanography and Paleoclimatology, 35(11), e2020PA004019, 2020b.

Telesiński, M. M., Spielhagen, R. F., and Bauch, H. A.: Water mass evolution of the Greenland Sea since late glacial times, Clim. Past, 10(1), 123-136, 2014a.

Telesiński, M. M., Spielhagen, R. F., and Lind, E. M.: A high-resolution Lateglacial and Holocene palaeoceanographic record from the Greenland Sea, Boreas, 43(2), 273-285, 2014b.

Thornalley, D. J., Elderfield, H., and McCave, I. N.: Holocene oscillations in temperature and salinity of the surface subpolar North Atlantic, Nature, 457(7230), 711-714, 2009.

Van Nieuwenhove, N., Pearce, C., Knudsen, M. F., Røy, H., and Seidenkrantz, M. S.: Meltwater and seasonality influence on Subpolar Gyre circulation during the Holocene, Palaeogeogr. Palaeocl., 502, 104-118, 2018.

Vare, L. L., Masse, G., Gregory, T. R., Smart, C. W., and Belt, S. T.: Sea ice variations in the central Canadian Arctic Archipelago during the Holocene, Quaternary Sci. Rev., 28, 1354–1366, 2009.

Vinje, T. E.: Sea Ice Conditions in the European Sector of the Marginal Seas of the Arctic 1966–75, 1975, Norwegian Polar Institut, 163–174, 1977.

Wangner, D. J., Jennings, A. E., Vermassen, F., Dyke, L. M., Hogan, K. A., Schmidt, S., Kjær, K. H., Knudsen, M. F., and Andresen, C. S.: A 2000-year record of ocean influence on Jakobshavn Isbræ calving activity, based on marine sediment cores, The Holocene, 28(11), 1731-1744, 2018.

Weatherall, P., Marks, K. M., Jakobsson, M., Schmitt, T., Tani, S., Arndt, J. E., Rovere, M., Chayes, D., Ferrini, V. and Wigley, R.: A new digital bathymetric model of the world's oceans, Earth and Space Science, 2(8), 331-345, 2015.

Werner, K., Spielhagen, R. F., Bauch, D., Hass, H. C., and Kandiano, E.: Atlantic Water advection versus sea-ice advances in the eastern Fram Strait during the last 9 ka: Multiproxy evidence for a two-phase Holocene, Paleoceanography, 28(2), 283-295, 2013.

Weiss, H.: 4.2 ka BP megadrought and the Akkadian collapse, in: Megadrought and Collapse: from early agriculture to Angkor, edited by: Weiss, H., Oxford University Press, Oxford, 93–160, 2017.

https://doi.org/10.5194/cp-2021-59
Preprint. Discussion started: 2 June 2021

Werner, K., Müller, J., Husum, K., Spielhagen, R. F., Kandiano, E. S., and Polyak, L.: Holocene sea subsurface and surface water masses in the Fram Strait–Comparisons of temperature and sea-ice reconstructions, Quaternary Sci. Rev., 147, 194-209, 2016.

Wilson, N. J. and Straneo, F.: Water exchange between the continental shelf and the cavity beneath Nioghalvfjerdsbræ (79 North Glacier), Geophys. Res. Lett., 42(18), 7648-7654, 2015.

Wollenburg, J. E. and Mackensen, A.: Living benthic foraminifera from the central Arctic Ocean: Faunal composition, standing stock and diversity, Mar. Micropaleontol., 34, 153–185, 1998.

Wollenburg, J. E. and Kuhnt, W.: The response of benthic foraminifers to carbon flux and primary production in the Arctic Ocean, Mar. Micropaleontol., 40(3), 189-231, 2000.

Zehnich, M., Spielhagen, R. F., Bauch, H. A., Forwick, M., Hass, H. C., Palme, T., Stein, R., and Syring, N.: Environmental variability off NE Greenland (western Fram Strait) during the past 10,600 years, The Holocene, 30(12), 1752-1766, 2020.